Advanced Physical Models and Numerical Methods for High Enthalpy and Plasma Flows Applied to Hypersonics

Thierry E. Magin
Michael G. Kapper

von Karman Institute for Fluid Dynamics
Aeronautics and Aerospace Department
Chaussee de Waterloo 72
Rhode-Saint-Genese, Belgium 1640

July 2011

Final Report for 16 June 2010 to 16 December 2010

REPORT DOCUMENTATION PAGE

Form Approved OMB No. 0704-0188

1. REPORT DATE *(DD-MM-YYYY)* 28-07-2011	2. REPORT TYPE Final Report	3. DATES COVERED *(From – To)* 16 June 2010 – 16 December 2010

4. TITLE AND SUBTITLE	5a. CONTRACT NUMBER
Advanced Physical Models and Numerical Methods for High Enthalpy and Plasma Flows Applied to Hypersonics	FA8655-10-1-3076

5b. GRANT NUMBER

Grant 10-3076

5c. PROGRAM ELEMENT NUMBER

61102F

6. AUTHOR(S) Thierry E. Magin Michael G. Kapper	5d. PROJECT NUMBER

5d. TASK NUMBER

5e. WORK UNIT NUMBER

7. PERFORMING ORGANIZATION NAME(S) AND ADDRESS(ES) von Karman Institute for Fluid Dynamics Aeronautics and Aerospace Department Chaussee de Waterloo 72 Rhode-Saint-Genese, Belgium 1640	8. PERFORMING ORGANIZATION REPORT NUMBER N/A

9. SPONSORING/MONITORING AGENCY NAME(S) AND ADDRESS(ES) EOARD Unit 4515 BOX 14 APO AE 09421	10. SPONSOR/MONITOR'S ACRONYM(S) AFRL/AFOSR/RSW (EOARD)
	11. SPONSOR/MONITOR'S REPORT NUMBER(S) **AFRL-AFOSR-UK-TR-2011-0023**

12. DISTRIBUTION/AVAILABILITY STATEMENT

Approved for public release; distribution is unlimited. (approval given by local Public Affairs Office)

13. SUPPLEMENTARY NOTES

14. ABSTRACT

This report results from a contract tasking von Karman Institute for Fluid Dynamics on modeling of high enthalpy flows. Collisional-Radiative models for the noble gases have been detailed which included atom and electron-impact processes as well as radiative processes. These models are intended to support plasmadynamic simulations under conditions of high non-equilibrium. The data has been presented in terms of angle-integrated cross sections where we have no assumption of the distribution function has been assumed. This leaves open the possibility to compute the CR rates using an arbitrary distribution function, including a bin approach.

While detailed validation has been provided for argon, results for krypton and xenon are still preliminary. Work is currently underway to increase the level of sophistication. These models will be refined and benchmarked against further experimental data, including expansion flows in which radiative processes dominate.

15. SUBJECT TERMS

EOARD, Hypersonic Flow, Plasma Aerodynamics

16. SECURITY CLASSIFICATION OF:			17. LIMITATION OF ABSTRACT	18, NUMBER OF PAGES	19a. NAME OF RESPONSIBLE PERSON Gregg Abate
a. REPORT UNCLAS	b. ABSTRACT UNCLAS	c. THIS PAGE UNCLAS	SAR	41	19b. TELEPHONE NUMBER *(Include area code)* +44 (0)1895 616021

Advanced Physical Models and Numerical Methods for High Enthalpy and Plasma Flows Applied to Hypersonics

Investigators: Prof. Thierry E. Magin (P. I.), Dr. Michael G. Kapper

magin@vki.ac.be

Aeronautics and Aerospace Department

von Karman Institute for Fluid Dynamics

Contents

1   Introduction

Modeling of high-enthalpy plasmas is essential to the fundamental understanding and development of many applications of interest to the Air Force, including aerodynamic flow control, re-entry and hypersonic air-breathing vehicles, as well as plasma discharges for electric propulsion devices. As applied to such cases, modeling can aid in improved aerodynamic performance, thermal protection systems, combustion enhancement, and thruster efficiency among others. The difficulty in modeling such plasmas is the high-degree of nonequilibrium between the various plasma components. Energy exchange rates between the various internal modes, for example, may be comparable to the transport time scales, necessitating multi-temperature and collisional-radiative (CR) models. Furthermore, momentum exchange between the various components may be slow requiring a multi-fluid description of the plasma. These complexities are further compounded when a continuum description of the plasma is no longer valid, making it necessary to augment traditional CFD approaches with kinetic or moment equations.

In a given flow field simulation, the plasma conditions can vary greatly, making it necessary to combine multiple descriptions of the plasma as determined by the local conditions, and in particular, the degree of nonequilibrium. For example, the plasma transport may transition between rarefied and continuum flow, requiring appropriate models for each case through hybrid techniques. Such hybridization can also be important to the chemistry of the flow. In the case of electronic excitation and ionization, detailed collisional-radiative models may be essential in accurately capturing the flow in certain regions, while unnecessary and otherwise computationally-burdensome in regions in which nonequilibrium effects become negligible. In such cases, a hybridization approach between a CR model along with a simple redistribution of levels according to a Boltzmann distribution where appropriate can yield significant performance gains.

In particular, it is desired to develop models based on a multi-temperature, multi-component description of the plasma combined with collisional-radiative models in order to describe the chemical kinetics. Recent research on shocktube simulations in monatomic gases has provided valuable insight into the kinetics and dynamics of the collisionally-dominated regime of the plasma. However, it is also important to investigate regimes in which radiative process can dominate collisional processes. One such example is where radiative recombination begins to dominate three-body recombination when there is a lack of third body collision partners.

The current work is focused on the development of CR models for monatomic gases. The models must be detailed enough to resolve the degree of nonequilibrium in the plasma while remaining robust and efficient enough to permit coupling with unsteady, multi-dimensional flow solvers. We first develop the models for argon, krypton and xenon and then validate them using shocktube data.

2 General model

We begin by describing a general CR model which is then applied specifically to Ar, Kr and Xe. Since detailed cross sections for all transitions are not known by either theoretical or experimental means, generalized models can provide useful approximations to otherwise unknown quantities. These semi-empirical models are validated on transitions where data are available and can thus provide trends and insights.

The processes considered can be represented by the following equations,

$$\text{Ar}(i) + \text{e}^- \underset{F_{ji}}{\overset{C_{ij}}{\rightleftharpoons}} \text{Ar}(j) + \text{e}^- \tag{1}$$

$$\text{Ar}(i) + \text{Ar}(1) \underset{L_{ji}}{\overset{K_{ij}}{\rightleftharpoons}} \text{Ar}(j) + \text{Ar}(1) \tag{2}$$

$$\text{Ar}(i) + \text{e}^- \underset{O_i}{\overset{S_i}{\rightleftharpoons}} \text{Ar}^+ + \text{e}^- + \text{e}^- \tag{3}$$

$$\text{Ar}(i) + \text{Ar}(1) \underset{W_i}{\overset{V_i}{\rightleftharpoons}} \text{Ar}^+ + \text{e}^- + \text{Ar}(1) \tag{4}$$

$$\text{Ar}(i) + h\nu_{ij} \underset{\Lambda_{ji} A_{ji}}{\rightleftharpoons} \text{Ar}(j) \tag{5}$$

$$\text{Ar}(i) + h\nu_i \underset{\Lambda_i R_i}{\rightleftharpoons} \text{Ar}^+ + \text{e}^- \tag{6}$$
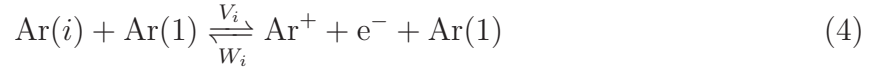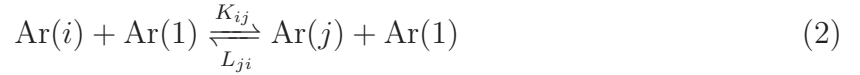
where the rate coefficients defined by [33] are summarized in Table 1. Although the processes in this section are expressed for argon, they are equally applicable for krypton and xenon. The convention adopted here is $j > i$ such that C_{ij} and K_{ij} represent the rates for excitation from level i to j while F_{ji}, L_{ji}, and Λ_{ji} are the rates for de-excitation from level j to i. The levels considered for the models presented herein include only those contained in the lowest lying manifolds, beyond which the ionization limit is approximately 1 eV or less. Thus the lower-lying states considered here make-up the bottleneck to the ionization regime and contain most of the energy of bound states. Note also that neutral atoms have two ionization potentials owing to the fact that the levels of argon are split according to two possible configurations for the core angular momentum j_c. As ionization and recombination can proceed only between levels having the same value of j_c, the two lowest lying levels of the corresponding ions must be accounted for individually. Thus in the current model, these two levels are treated as separate species and convected as such.

2.1 Atom impact processes

Heavy-particle impact cross sections are scarce in the literature, requiring us to rely upon semi-empirical models including that of Drawin [19]. However, caution must be exercised when using such models as are known to over-estimate the impact cross sections by at least an order of magnitude [10]. In several applications of general interest, including shock-heated plasma, atom-atom collisions are the only means for initial electron production and yield the priming electrons that eventually trigger inelastic electron collisions. Excitation from ground state in particular plays a significant role in determining the time necessary

Rate Coefficient	Process
C_{ij}	collisional excitation by electrons
K_{ij}	collisional excitation by ground state atoms
F_{ji}	collisional de-excitation by electrons
L_{ji}	collisional de-excitation by ground state atoms
S_i, V_i	collisional ionization
O_i, W_i	three-body recombination
R_i	radiative recombination
A_{ij}	transition probability/spontaneous emission (Einstein coefficient)
Λ_{ij}	bound-bound optical escape factor
Λ_i	bound-free optical escape factor
k_{ei}	electron-ion collisions
k_{en}	electron-neutral collisions
k_{brems}	bremsstrahlung emission

Table 1: Summary of rate coefficients for collisional-radiative model.

for the onset of an electron avalanche behind a viscous shock for example. Starting with Drawin's formula

$$\sigma_{ij}^a(\varepsilon) = 4\pi a_\circ^2 \left(\frac{I_H}{\varepsilon_{ij}}\right)^2 \frac{m_{Ar}}{m_H} \xi^2 f_{ij} \frac{2m_e}{m_{Ar} + m_e} \frac{\varepsilon/\Delta\varepsilon_{ij} - 1}{\left(1 + \frac{2m_e}{m_{Ar}+m_e}(\varepsilon/\Delta\varepsilon_{ij} - 1)\right)^2} \tag{7}$$

where I_H is the ionization potential of the hydrogen atom, $a_\circ$ is the Bohr radius and $\xi = 6$ is the number of optical electrons of argon. For the energy ranges under consideration, Eq. (7) is well-approximated by a linear function,

$$\sigma_{1j}^a(\varepsilon) = \beta_{1j}^*(\varepsilon - \Delta\varepsilon_{ij}), \tag{8}$$

where

$$\beta_{1j}^* = 4\pi a_\circ^2 \frac{(I_H)^2}{\varepsilon_{ij}^3} \xi^2 f_{ij} \frac{2m_e}{m_H} \tag{9}$$

and f_{ij} is the oscillator strength of the transition.

Less sensitive are the ionization cross sections. The formula of Drawin (Eq. (7), replacing $f_{ij} = 1$ and $\varepsilon_{ij} = I_i$, the ionization potential) can be used to obtain the cross sections for ionization for the excited levels[1],

$$\sigma_i^a(\varepsilon) = 4\pi a_\circ^2 \left(\frac{I_H}{I_i}\right)^2 \frac{m_{Ar}}{m_H} \xi^2 \frac{2m_e}{m_{Ar} + m_e} \frac{\varepsilon/I_i - 1}{\left(1 + \frac{2m_e}{m_{Ar}+m_e}(\varepsilon/I_i - 1)\right)^2}. \tag{10}$$

---

[1] for further details, the reader is directed to [4] and [33] and the references therein

2.2   Electron impact excitation

Zatsarinny & Bartschat [35] have published cross sections using R-matrix calculations for most of the noble gases which agree favorably with the detailed experimental results of Buckmann $et\ al$ [3]. Recent experiments by have provided further validation of the R-matrix calculations. For transitions for which such detailed computations are not yet available, the formula of Drawin,

$$\sigma_{ij}^e(\varepsilon) = 4\pi a_\circ^2 \frac{(u_{ij}-1)}{u_{ij}^2} \begin{cases} \alpha_{ij}^A f_{ij}\left(I_H/\varepsilon_{ij}\right)^2 \ln(1.25\beta_{ij}u_{ij}) \\ \alpha_{ij}^P \\ \alpha_{ij}^S (u_{ij}+1)/u_{ij}^3 \end{cases} \tag{11}$$

may be used with $\alpha_{ij}^A f_{ij} = 1$, $\alpha_{ij}^P = 1$, and $\alpha_{ij}^S = 1$.

2.3   Electron impact ionization

For electron impact cross sections, we rely upon the Deutsch-Märk formalism [6] which combines a semi-empirical Gryzinski-type energy dependence of the cross section with quantum mechanically calculated molecular structure information. The cross sections can be expressed as

$$\sigma_i(\varepsilon) = g_{n\ell}\pi r_{n\ell}^2 \xi_{n\ell} f(\varepsilon), \tag{12}$$

where $g_{n\ell}$ are the reduced weighting factors, $r_{n\ell}$ are the radii of the valence electron (n, ℓ are the principal and orbital quantum numbers describing the electronic state), and

$$f_i(\varepsilon) = d\frac{I_i}{\varepsilon}\left(\frac{\varepsilon/I_i-1}{\varepsilon/I_i+1}\right)^a\left[b + c\left(1 - \frac{I_i}{2\varepsilon}\right)\ln(2.7 + (\varepsilon/I_i-1)^{1/2})\right]. \tag{13}$$

the

2.4   Elastic collisions

Mitroy [25] used modified effective range theory (MERT) to develop a semi-empirical fit for momentum transfer cross sections involving noble gases, both pure as well as in

Atom	Polarizability	
	Dipole, α_d $[a_\circ^3]$	Quadrupole, α_q $[a_\circ^5]$
Ne	2.69	7.52
Ar	11.07	52.25
Kr	17.06	97.39
Xe	27.66	209.85

Table 2: Dipole and quadrupole polarizabilities of the noble gases ([28]).

mixtures with H_2. According to the theory, the cross section can be expressed in terms of the phase shifts for the partial waves which are given by

$$\tan \eta_0 = -Ak[1 + (4\alpha_d/3)k^2 \ln k] - (\pi\alpha_d/3)k^2 + Dk^3 + Fk^4 \tag{14}$$

$$\tan \eta_1 = a_1\alpha_d k^2 - A_1 k^3 + (b_1\alpha_d^2 + c_1\alpha_q^2)k^4 + Hk^5 \tag{15}$$

$$\tan \eta_2 = a_2\alpha_d k^2 - (b_2\alpha_d^2 + c_2\alpha_q^2)k^4 + A_2 k^5 \tag{16}$$

$$\tan \eta_\ell = a_\ell\alpha_d k^2 + (b_\ell\alpha_d^2 + c_\ell\alpha_q)k^4 \tag{17}$$

$$\tag{18}$$

where ℓ is the electron angular momentum number. The coefficients a_ℓ, b_ℓ and c_ℓ are given by

$$a_\ell = \frac{\pi}{(2\ell + 3)(2\ell + 1)(2\ell - 1)} \tag{19}$$

$$b_\ell = \frac{\pi[15(2\ell + 1)^4 - 140(2\ell + 1)^2 + 128]}{[(2\ell + 3)(2\ell + 1)(2\ell - 1)]^3(2\ell + 5)(2\ell - 3)} \tag{20}$$

$$c_\ell = \frac{3a_\ell}{(2\ell + 5)(2\ell - 3)}. \tag{21}$$

$$\tag{22}$$

In terms of the phase shifts, the momentum transfer cross section is given by

$$\sigma_{\mathrm{M}} = \frac{4\pi}{k^2} \sum_\ell (\ell + 1) \sin^2(\eta_\ell - \eta_{\ell+1}). \tag{23}$$

The dipole α_d and quadrupole α_q polarizabilities for the noble gases are summarized in Table 2.4.

2.5 Photorecombination/Photoionization

We start with photorecombination, which can play an important role in radiative cooling. The cross section for photorecombination can be found from the cross section for photoionization under equilibrium conditions (Zel'dovich & Raizer [37]),

$$\sigma_{c,i}(\nu) = \frac{g_n}{g_+} \frac{h^2\nu^2}{m_e^2 v_e^2 c^2} \sigma_{\nu,i}(\nu). \tag{24}$$

Utilizing the relation $h\nu = m_e v^2/2 + \varepsilon_i = \varepsilon + \varepsilon_i$, the cross section associated with the ground state is given by

$$\sigma_{\nu,1}(\varepsilon) = \frac{g_1}{g_+} \frac{(\varepsilon + \varepsilon_1)^2}{2\varepsilon m_e c^2}$$

$$\times \begin{cases} 3.5 \times 10^{-21} & 0 \leq \varepsilon \leq 2I_H - \varepsilon_1 \\ 2.8 \times 10^{-20} \left(\frac{I_H}{\varepsilon + \varepsilon_1}\right)^3 & \varepsilon > 2I_H - \varepsilon_1 \end{cases} \tag{25}$$

while all others are computed using

$$\sigma_{\nu,i}(\varepsilon) = \gamma_i \frac{g_i}{g_+} \frac{(\varepsilon + \varepsilon_i)^2}{2\varepsilon m_e c^2} 10^{-22}$$

$$\times \begin{cases} 2 & 0 \leq \varepsilon \leq 0.59 I_H - \varepsilon_1 \\ 7.91 \left(\dfrac{\varepsilon_i}{I_H}\right)^{\frac{5}{2}} \left(\dfrac{I_H}{\varepsilon + \varepsilon_i}\right)^3 & \varepsilon > 0.59 I_H - \varepsilon_i \end{cases} \qquad (26)$$

2.6   Bound-bound transitions

Bound-bound transitions are another significant source of radiative cooling of the plasma. The photo-absorption cross section for a given bound-bound transition may be estimated by (Zel'dovich & Raizer),

$$\sigma_{ij} = \frac{1}{\nu_{ij}} \int \sigma_{\nu,ij} \, d\nu = 2.65 \times 10^{-6} \frac{f_{ij}^{\mathrm{abs}}}{\nu_{ij}} \; [\mathrm{m}^2] \qquad (27)$$

where the absorption oscillator strength is given by

$$f_{ij}^{\mathrm{abs}} = \frac{g_j}{g_i} \frac{A_{ji}}{3\gamma}. \qquad (28)$$

Contributions to the parameter γ have been assumed to result from a combination of natural and pressure line broadening,

$$\gamma = \gamma_{\mathrm{nat}} + \gamma_{\mathrm{col}} \qquad (29)$$

given by

$$\gamma_{\mathrm{nat}} = \frac{8\pi^2 e^2 \nu^2}{3mc^3} = 2.47 \times 10^{-22} \nu^2 \; [\mathrm{s}^{-1}] \qquad (30)$$

and

$$\gamma_{\mathrm{col}} = \frac{2}{\tau_{\mathrm{col}}} = 2\sigma \bar{v} n \qquad (31)$$

respectively. Based on the resulting mean-free paths, it has been assumed that all bound-bound radiation to the ground level from the excited states is absorbed. For all other transitions, the mean-free path is several orders of magnitude greater than the dimensions of the shock tube and the associated radiation is assumed to escape.

2.7   Bremsstrahlung emission

Free-free transitions have been incorporated in the model via Kramer's formula [37] for *Bremsstrahlung* emission. Thus the corresponding term in the vector of source terms is:

$$\left[\frac{dE_e}{dt}\right]_{\mathrm{CR}} = -\frac{16\pi^2}{3\sqrt{3}} \frac{\bar{v}_e Z_{\mathrm{eff}}^2 e^6 \bar{g}}{m_e h (4\pi\varepsilon_\circ c)^3} n_+ n_e \qquad (32)$$

$$= -1.42 \times 10^{-40} Z_{\mathrm{eff}}^2 T_e^{1/2} n_+ n_e \; [\mathrm{J/m}^3 \cdot \mathrm{s}]$$

where $\bar{g}$ is the gaunt factor (here taken to be unity) and the effective charge Z_{eff}^2 is taken to be 1.67 to better match the experimental conditions given by Glass & Liu [12]. Bremsstrahlung emission resulting from neutral atoms is 1–2 orders of magnitude less than for ions and has therefore been neglected [37]. The plasma is assumed to be optically thin to all Bremsstrahlung emission.

2.8 Model reduction

Since computational costs increase exponentially with the addition of more states, solving fully detailed CR models quickly becomes intractable, especially when coupled with multidimensional CFD codes. For this reason, it is necessary to develop reduced CR models from which accurate kinetics can still be recovered for the conditions of interest. The reduced models must be benchmarked against the most detailed models available to ensure their validity.

3 Argon

Due to its relative abundance, argon has been extensively used in experimental investigations of plasma gas dynamics. Shocktube experiments in particular have been used to validate CR models (c.f. [24, 23, 20, 27, 14]). But perhaps the most significant work was carried out at the Institute of Aerospace Sciences at the University of Toronto (UTIAS) in which unsteady effects were discovered to be a further characteristic of hypervelocity shocks in argon (c.f. [2, 13, 12]). This was taken advantage of by Cambier [5] who showed that galloping instabilities of the shock front could in fact be explained through the influence of the kinetics of excitation and ionization on the transport of the gas. Subsequent work by Kapper & Cambier [17, 18] extended the sophistication of the CR model and were able to reproduce the unsteady shock structure in two-dimensional space. That model is reiterated here and serves as the foundation for extension to krypton and xenon.

3.0.1 Atom impact processes

For atom-impact excitation of argon, we have used Drawin's formula (Eq. (8)) for the allowed transitions. The inner $3p^54s$ manifold transitions, however, take the form [4]

$$\sigma_{ij}^a(\varepsilon) = \beta_{ij}^* \frac{\varepsilon - \varepsilon_{ij}}{\varepsilon_{ij[eV]}^{2.26}} \tag{33}$$

where $\varepsilon_{ij[eV]}$ is the transition energy in eV. The linear β-parameters are provided in Tables 3.0.1 and 3.0.1. Note the relative strength of $\Delta j_c \equiv 0$ transitions compared to the $4s$–$4s'$ ($\Delta j_c n_e 0$) transition.

For atom-impact ionization, the cross section for ionization from ground state argon is taken from Haugsjaa and Amme [15],

$$\sigma_1^a(\varepsilon) = 1.8 \times 10^{-25}(\varepsilon_{[eV]} - 15.760)^{1.3} \text{ [m}^2\text{]}, \tag{34}$$

while the formula of Drawin (Eq. 10) has been used for the excited states.

i	$\varepsilon(i)$ [eV]	g_i	j_c	$n\ell[K]_J$	i	$\varepsilon(i)$ [eV]	g_i	j_c	$n\ell[K]_J$
1	0	1	1.5	$[\mathrm{Mg}]3p^6$	42	14.711	3	1.5	$4d[1/2]_1$
2	11.548	5	1.5	$4s[3/2]_2$	43	14.738	1	0.5	$5p'[1/2]_0$
3	11.624	3	1.5	$4s[3/2]_1$	44	14.743	5	1.5	$4d[3/2]_2$
4	11.723	1	0.5	$4s'[1/2]_0$	45	14.757	9	1.5	$4d[7/2]_4$
5	11.828	3	0.5	$4s'[1/2]_1$	46	14.781	7	1.5	$4d[7/2]_3$
6	12.907	3	1.5	$4p[1/2]_1$	47	14.809	5	1.5	$4d[5/2]_2$
7	13.076	7	1.5	$4p[5/2]_3$	48	14.824	7	1.5	$4d[5/2]_3$
8	13.095	5	1.5	$4p[5/2]_2$	49	14.839	5	1.5	$6s[3/2]_2$
9	13.153	3	1.5	$4p[3/2]_1$	50	14.848	3	1.5	$6s[3/2]_1$
10	13.172	5	1.5	$4p[3/2]_2$	51	14.859	3	1.5	$4d[3/2]_1$
11	13.273	1	1.5	$4p[1/2]_0$	52	14.901	3	1.5	$4f[3/2]_1$
12	13.283	3	0.5	$4p'[3/2]_1$	53	14.901	5	1.5	$4f[3/2]_2$
13	13.302	5	0.5	$4p'[3/2]_2$	54	14.904	11	1.5	$4f[9/2]_5$
14	13.328	3	0.5	$4p'[1/2]_1$	55	14.904	9	1.5	$4f[9/2]_4$
15	13.480	1	0.5	$4p'[1/2]_0$	56	14.907	7	1.5	$4f[5/2]_3$
16	13.845	1	1.5	$3d[1/2]_0$	57	14.907	5	1.5	$4f[5/2]_2$
17	13.864	3	1.5	$3d[1/2]_1$	58	14.909	7	1.5	$4f[7/2]_3$
18	13.903	5	1.5	$3d[3/2]_2$	59	14.909	9	1.5	$4f[7/2]_4$
19	13.979	9	1.5	$3d[7/2]_4$	60	14.953	5	0.5	$4d'[3/2]_2$
20	14.013	7	1.5	$3d[7/2]_3$	61	14.955	5	0.5	$4d'[5/2]_2$
21	14.063	5	1.5	$3d[5/2]_2$	62	14.972	7	0.5	$4d'[5/2]_3$
22	14.068	5	1.5	$5s[3/2]_2$	63	15.004	3	0.5	$4d'[3/2]_1$
23	14.090	3	1.5	$5s[3/2]_1$	64	15.011	3	1.5	$6p[1/2]_1$
24	14.099	7	1.5	$3d[5/2]_3$	65	15.014	1	0.5	$6s'[1/2]_0$
25	14.153	3	1.5	$3d[3/2]_1$	66	15.022	3	0.5	$6s'[1/2]_1$
26	14.214	5	0.5	$3d'[5/2]_2$	67	15.023	7	1.5	$6p[5/2]_3$
27	14.234	5	0.5	$3d'[3/2]_2$	68	15.026	5	1.5	$6p[5/2]_2$
28	14.236	7	0.5	$3d'[5/2]_3$	69	15.034	3	1.5	$6p[3/2]_1$
29	14.241	1	0.5	$5s'[1/2]_0$	70	15.036	5	1.5	$6p[3/2]_2$
30	14.255	3	0.5	$5s'[1/2]_1$	71	15.060	1	1.5	$6p[1/2]_0$
31	14.304	3	0.5	$3d'[3/2]_1$	72	15.083	7	0.5	$4f'[7/2]_3$
32	14.464	3	1.5	$5p[1/2]_1$	73	15.083	9	0.5	$4f'[7/2]_4$
33	14.499	7	1.5	$5p[5/2]_3$	74	15.083	7	0.5	$4f'[5/2]_3$
34	14.506	5	1.5	$5p[5/2]_2$	75	15.083	5	0.5	$4f'[5/2]_2$
35	14.525	3	1.5	$5p[3/2]_1$	76	15.101	1	1.5	$5d[1/2]_0$
36	14.529	5	1.5	$5p[3/2]_2$	77	15.118	3	1.5	$5d[1/2]_1$
37	14.576	1	1.5	$5p[1/2]_0$	78	15.131	9	1.5	$5d[7/2]_4$
38	14.681	3	0.5	$5p'[3/2]_1$	79	15.137	5	1.5	$5d[3/2]_2$
39	14.687	3	0.5	$5p'[1/2]_1$	80	15.146	7	1.5	$5d[7/2]_3$
40	14.688	5	0.5	$5p'[3/2]_2$	∞	15.760	4	1.5	$[\mathrm{Mg}]3p^5$
41	14.694	1	1.5	$4d[1/2]_0$	∞'	15.937	2	0.5	$[\mathrm{Mg}]3p^5$

Table 3: Lowest 80 levels of Ar I by energy.

i	j	β_{ij}^* [m^2/eV]	f_{ij}
$3p^6$	$3d'[3/2]_1$	9.24×10^{-24}	1.06×10^{-01}
$3p^6$	$3d[3/2]_1$	8.38×10^{-24}	9.32×10^{-02}
$3p^6$	$4s'[1/2]_1$	3.85×10^{-23}	2.50×10^{-01}
$3p^6$	$4s[3/2]_1$	9.89×10^{-24}	6.09×10^{-02}
$3p^6$	$5s'[1/2]_1$	1.05×10^{-24}	1.19×10^{-02}
$3p^6$	$5s[3/2]_1$	2.46×10^{-24}	2.70×10^{-02}
$4s'[1/2]_0$	$4p'[1/2]_1$	5.38×10^{-22}	3.14×10^{-01}
$4s'[1/2]_0$	$4p'[3/2]_1$	9.88×10^{-22}	5.29×10^{-01}
$4s'[1/2]_0$	$4p[1/2]_1$	2.05×10^{-22}	4.80×10^{-02}
$4s'[1/2]_0$	$4p[3/2]_1$	1.99×10^{-22}	8.22×10^{-02}
$4s'[1/2]_1$	$4p'[1/2]_0$	1.96×10^{-22}	1.25×10^{-01}
$4s'[1/2]_1$	$4p'[1/2]_1$	3.30×10^{-22}	1.57×10^{-01}
$4s'[1/2]_1$	$4p'[3/2]_1$	3.48×10^{-22}	1.51×10^{-01}
$4s'[1/2]_1$	$4p'[3/2]_2$	8.71×10^{-22}	3.94×10^{-01}
$4s'[1/2]_1$	$4p[1/2]_1$	2.14×10^{-23}	3.80×10^{-03}
$4s'[1/2]_1$	$4p[3/2]_1$	4.23×10^{-23}	1.39×10^{-02}
$4s'[1/2]_1$	$4p[3/2]_2$	3.12×10^{-22}	1.07×10^{-01}
$4s'[1/2]_1$	$4p[5/2]_2$	1.23×10^{-22}	3.52×10^{-02}
$4s[3/2]_1$	$4p'[1/2]_0$	5.82×10^{-25}	5.26×10^{-04}
$4s[3/2]_1$	$4p'[1/2]_1$	2.07×10^{-23}	1.45×10^{-02}
$4s[3/2]_1$	$4p'[3/2]_1$	2.79×10^{-25}	1.80×10^{-04}
$4s[3/2]_1$	$4p'[3/2]_2$	1.72×10^{-22}	1.15×10^{-01}
$4s[3/2]_1$	$4p[1/2]_0$	1.80×10^{-22}	1.14×10^{-01}
$4s[3/2]_1$	$4p[1/2]_1$	2.55×10^{-22}	7.60×10^{-02}
$4s[3/2]_1$	$4p[3/2]_1$	4.95×10^{-22}	2.50×10^{-01}
$4s[3/2]_1$	$4p[3/2]_2$	1.50×10^{-22}	7.85×10^{-02}
$4s[3/2]_1$	$4p[5/2]_2$	8.47×10^{-22}	3.81×10^{-01}
$4s[3/2]_2$	$4p'[1/2]_1$	3.51×10^{-23}	2.79×10^{-02}
$4s[3/2]_2$	$4p'[3/2]_1$	3.90×10^{-24}	2.87×10^{-03}
$4s[3/2]_2$	$4p'[3/2]_2$	3.74×10^{-23}	2.85×10^{-02}
$4s[3/2]_2$	$4p[1/2]_1$	4.01×10^{-22}	1.42×10^{-01}
$4s[3/2]_2$	$4p[3/2]_1$	4.76×10^{-23}	2.78×10^{-02}
$4s[3/2]_2$	$4p[3/2]_2$	3.54×10^{-22}	2.14×10^{-01}
$4s[3/2]_2$	$4p[5/2]_2$	1.71×10^{-22}	8.94×10^{-02}
$4s[3/2]_2$	$4p[5/2]_3$	9.10×10^{-22}	4.58×10^{-01}

Table 4: Atom impact excitation parameters for allowed transitions from ground state Ar.
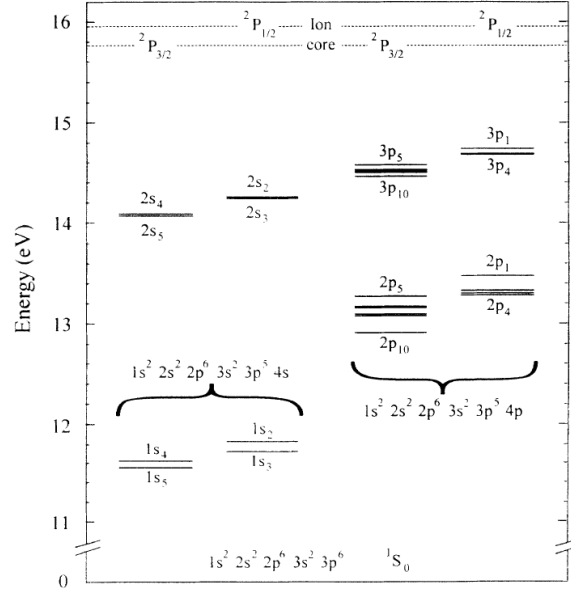
Figure 1: Partial Grotrian diagram for neutral argon taken from [30].

i	j	β_{ij}^* [m^2/eV]
$4s[3/2]_2$	$4s[3/2]_1$	1.79×10^{-24}
$4s[3/2]_2$	$4s'[1/2]_0$	4.80×10^{-26}
$4s[3/2]_2$	$4s'[1/2]_1$	4.80×10^{-26}
$4s[3/2]_1$	$4s'[1/2]_0$	4.80×10^{-26}
$4s[3/2]_1$	$4s'[1/2]_1$	4.80×10^{-26}
$4s'[1/2]_0$	$4s'[1/2]_1$	1.79×10^{-24}

Table 5: Atom impact excitation parameters for intra-$4s$ transitions.

3.1   Electron impact processes

Zatsarinny & Bartschat [35] have performed R-matrix calculations to obtain highly detailed cross sections for electron impact excitation of argon near threshold energies. These have been provided for all inter-level transitions up to the $3d$ and $5s$ manifolds. Beyond this, Drawin's formula has been used systematically.

For ionization from the excited states, we have utilized the Deutsch-Märk formalism as previously mentioned. The necessary parameters for Eqs. (12) and (13) are given in Table 3.1, while the resulting cross sections have been plotted in Figure 2. For ionization from the excited states we have considered the electron occupying the valence shell only. For ionization from the core, we have considered contributions form all sub-shells. For ionization from the core, we have have compared the cross sections from the DM formalism with the experimental fit of Straub et al [32].

3.2   Elastic collisions

The theoretical cross section of McEachran & Stauffer [21] have been utilized for the elastic momentum transfer cross sections between neutral argon and electrons, which are reproduced in Table 3.2 and plotted in Figure 3.

3.3   Photorecombination/Photoionization

For argon, the parameter γ_i in Eq. (26) takes the values 0.0763, 0.0458, 0.0305, and 0.0915 for $i = 2$, 3, 4, and 5, respectively [33]. Based on nominal shock tube plasma conditions, an estimation of the mean-free path for photoionization from the ground state is on the order of 100 μm. In the case of the $4s$ levels, their lower populations combined with reduced cross sections result in mean-free paths on the order of 1 m. Consequently, free-bound radiation into the ground state is assumed to be locally absorbed, while the plasma is assumed to be optically thin to transitions from the excited levels.

Valence electron shell, $n\ell$	$r_{n\ell}$ [Å]	$g_{n\ell} \times I_{n\ell}$ [eV]
$4s$	2.49	7.40
$5s$	6.35	6.35
$4p$	3.40	31.00
$3d$	4.36	13.60

Table 6: Radii of Ar valence electron and reduced weighting factors for $\xi = 1$ as taken from [8] and [6].
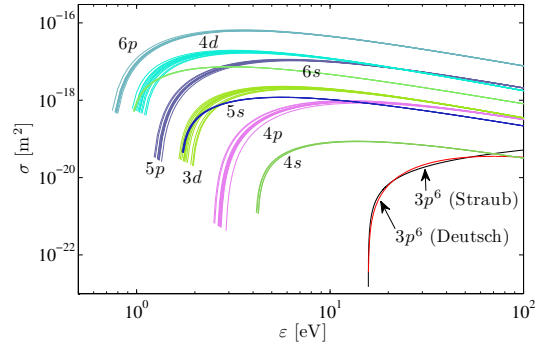
Figure 2: Ionization cross sections due to electron impact for Ar I as computed by the Deutsch-Märk formalism.

ε [eV]	σ_{en} [10^{20} m^2]	ε [eV]	σ_{en} [10^{20} m^2]
0.01	4.0231	0.41	0.3396
0.03	2.3425	0.51	0.5349
0.05	1.5247	0.61	0.7381
0.07	1.0261	0.71	0.9318
0.09	0.6998	0.81	1.1139
0.13	0.3291	0.91	1.2835
0.17	0.1599	1.00	1.4280
0.19	0.1198	1.50	2.1438
0.21	0.0983	2.00	2.8318
0.23	0.0917	3.00	4.4046
0.25	0.0969	4.00	6.3502
0.29	0.1316	5.00	8.6317
0.31	0.1573	7.50	14.6559
0.32	0.1724	10.00	17.8325

Table 7: Momentun transfer cross sections for electron-neutral collisions [21].

Figure 3: Momentum transfer cross sections for Ar I.

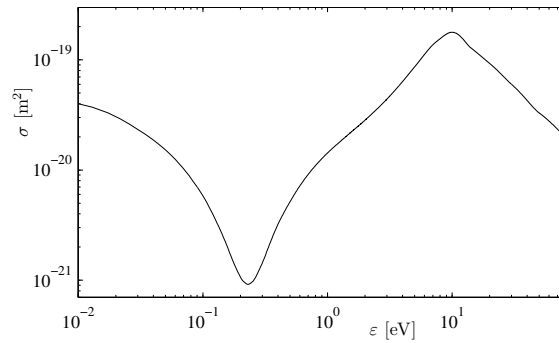| lower level	upper level	mean-free path [m]
$3p^6$	$4s[3/2]_1$	3.59×10^{-2}
$3p^6$	$4s'[1/2]_1$	9.47×10^{-3}
$3p^6$	$3d[1/2]_1$	2.41
$3p^6$	$5s[3/2]_1$	7.11×10^{-2}
$3p^6$	$3d[3/2]_1$	2.54×10^{-2}
$3p^6$	$5s'[1/2]_1$	1.34×10^{-1}
$3p^6$	$3d'[3/2]_1$	3.05×10^{-2}

Table 8: Estimated mean-free paths for bound-bound transitions to ground state for $T = 1$ eV and $n_{3p^6} = 10^{24}$ m^{-3}.

3.4 Bound-bound transitions

Bound-bound transitions are another significant source of radiative cooling of the plasma. The photo-absorption cross section for a given bound-bound transition may be estimated by [37],

$$\sigma_{ij} = \frac{1}{\nu_{ij}} \int \sigma_{\nu,ij} \, d\nu = 2.65 \times 10^{-6} \frac{f_{ij}^{\text{abs}}}{\nu_{ij}} \; [\text{m}^2] \tag{35}$$

where the absorption oscillator strength is given by

$$f_{ij}^{\text{abs}} = \frac{g_j}{g_i} \frac{A_{ji}}{3\gamma}. \tag{36}$$

For argon, we have estimated the contributions to the parameter γ in Eq. 28 by assuming a combination of natural and pressure line broadening,

$$\gamma = \gamma_{\text{nat}} + \gamma_{\text{col}} \tag{37}$$

given by

$$\gamma_{\text{nat}} = \frac{8\pi^2 e^2 \nu^2}{3mc^3} = 2.47 \times 10^{-22} \nu^2 \; [\text{s}^{-1}] \tag{38}$$

and

$$\gamma_{\text{col}} = \frac{2}{\tau_{\text{col}}} = 2\sigma \bar{v} n \tag{39}$$

respectively. The collision time τ_{col} and the collision cross section σ have been tallied for all argon-argon collisions. The radiation cross sections Eq. (35) have been estimated using the oscillator strengths and transition probabilities from Ralchenko *et al* [29] along with representative plasma conditions of the shock tube experiments. The resulting mean-free paths for bound-bound transitions to ground state given in Table VII are below the length scales of the shock tube dimensions and induction length for most of the levels.

3.5   Validation

This current model has been extensively benchmarked in the case of shock-heated argon plasma. Results obtained by Kapper & Cambier are shown in Figure 4. A detailed analysis of the results are provided within.

4   Krypton

Beyond argon, the heavier noble gases including krypton and xenon present a considerable challenge to theoretical computation of oscillator strengths and subsequent particle impact cross sections. The significant influence of relativistic effects means that models developed for lighter species have been unsuccessful in obtaining quantitative agreement. Despite this, active progress is being made in extending the models that will greatly benefit our CR models.

The lowest 80 levels of Kr I as given by NIST are listed in Table 9. Note that the energy needed to excite an electron to the lowest manifold is approximately 1.5 eV lower than that or Ar I, with subsequent ionization requiring an additional 4 eV, similar to argon. This translates to higher ionization fractions behind the shock.

4.0.1   Atom impact processes

For excitation due to heavy particle impact, the formula of Drawin (Eq. 8) has been used to obtain cross sections for the allowed transitions. The parameters β_{ij}^* are provided in Table 4.0.1.

4.1   Electron impact processes

Building upon their success for electron-impact excitation cross sections for argon, [36] have extended their calculations to krypton and xenon. The computed cross sections reproduced in Figures 10 and 11 show good agreement with high-resolution experiments near threshold for transitions to the $5s$ manifold from the ground state.

For ionization from the excited states, we have used the Deutsch-Märk formalism and have considered the electron in the valence shell only since this leads to better agreement with experimental data [7]. For ionization from the core, we have considered only the $5s$ sub-shell. The resulting cross sections have been plotted in Figure 6.

4.2   Elastic collisions

The momentum transfer cross sections for elastic impact of electrons with krypton have been given by Mitroy [25] for energies up to 1 eV. Beyond this, we have used the cross sections of McEachran & Stauffer [22]. The resulting cross sections are plotted in Figure 7.
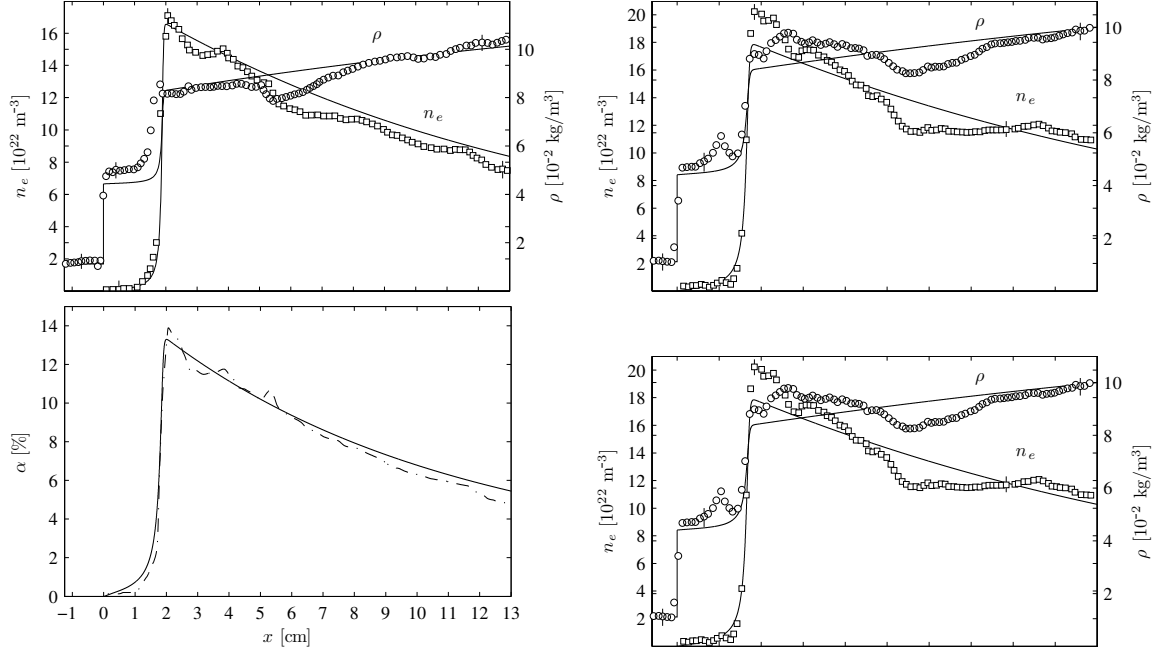
Figure 4: Heavy particle mass density and electron number density profiles (*top*) and ionization fractions (*bottom*) behind Mach 15.9 (*left*) and Mach 16.1 (*right*) shocks in pure argon. Results shown have been obtained considering excited levels from the $4s$, $4p$, $5s$, and $3d$ manifolds.
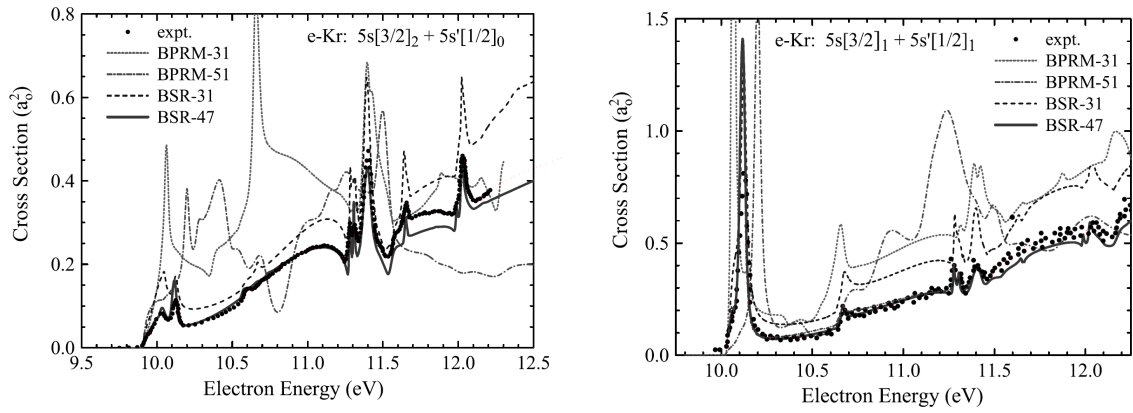

Figure 5: Electron-impact excitation cross sections for krypton taken from [36].

i	$\varepsilon(i)$ [eV]	g_i	j_c	$n\ell[K]_J$	i	$\varepsilon(i)$ [eV]	g_i	j_c	$n\ell[K]_J$
1	0	1	1.5	$[\mathrm{Zn}]4p^6$	42	13.036	3	0.5	$6s'[1/2]_1$
2	9.915	5	1.5	$5s[3/2]_2$	43	13.039	5	1.5	$5d[5/2]_2$
3	10.032	3	1.5	$5s[3/2]_1$	44	13.044	7	1.5	$5d[5/2]_3$
4	10.562	1	0.5	$5s'[1/2]_0$	45	13.099	5	1.5	$7s[3/2]_2$
5	10.644	3	0.5	$5s'[1/2]_1$	46	13.099	3	1.5	$5d[3/2]_1$
6	11.303	3	1.5	$5p[1/2]_1$	47	13.114	3	1.5	$7s[3/2]_1$
7	11.443	7	1.5	$5p[5/2]_3$	48	13.138	3	1.5	$4f[3/2]_1$
8	11.445	5	1.5	$5p[5/2]_2$	49	13.138	5	1.5	$4f[3/2]_2$
9	11.526	3	1.5	$5p[3/2]_1$	50	13.141	9	1.5	$4f[9/2]_4$
10	11.546	5	1.5	$5p[3/2]_2$	51	13.141	11	1.5	$4f[9/2]_5$
11	11.666	1	1.5	$5p[1/2]_0$	52	13.145	7	1.5	$4f[5/2]_3$
12	11.998	1	1.5	$4d[1/2]_0$	53	13.145	5	1.5	$4f[5/2]_2$
13	12.037	3	1.5	$4d[1/2]_1$	54	13.148	7	1.5	$4f[7/2]_3$
14	12.100	3	0.5	$5p'[3/2]_1$	55	13.148	9	1.5	$4f[7/2]_4$
15	12.112	5	1.5	$4d[3/2]_2$	56	13.267	3	1.5	$7p[1/2]_1$
16	12.125	9	1.5	$4d[7/2]_4$	57	13.284	5	1.5	$7p[5/2]_2$
17	12.140	3	0.5	$5p'[1/2]_1$	58	13.284	7	1.5	$7p[5/2]_3$
18	12.144	5	0.5	$5p'[3/2]_2$	59	13.294	3	1.5	$7p[3/2]_1$
19	12.179	7	1.5	$4d[7/2]_3$	60	13.297	5	1.5	$7p[3/2]_2$
20	12.256	1	0.5	$5p'[1/2]_0$	61	13.317	1	1.5	$7p[1/2]_0$
21	12.258	5	1.5	$4d[5/2]_2$	62	13.341	1	1.5	$6d[1/2]_0$
22	12.284	7	1.5	$4d[5/2]_3$	63	13.350	3	1.5	$6d[1/2]_1$
23	12.352	5	1.5	$6s[3/2]_2$	64	13.363	9	1.5	$6d[7/2]_4$
24	12.355	3	1.5	$4d[3/2]_1$	65	13.365	5	1.5	$6d[3/2]_2$
25	12.385	3	1.5	$6s[3/2]_1$	66	13.375	7	1.5	$6d[7/2]_3$
26	12.756	3	1.5	$6p[1/2]_1$	67	13.389	5	1.5	$6d[5/2]_2$
27	12.785	7	1.5	$6p[5/2]_3$	68	13.396	7	1.5	$6d[5/2]_3$
28	12.785	5	1.5	$6p[5/2]_2$	69	13.422	3	1.5	$6d[3/2]_1$
29	12.803	5	0.5	$4d'[3/2]_2$	70	13.431	5	1.5	$8s[3/2]_2$
30	12.809	3	1.5	$6p[3/2]_1$	71	13.437	3	1.5	$8s[3/2]_1$
31	12.815	5	1.5	$6p[3/2]_2$	72	13.445	3	0.5	$6p'[3/2]_1$
32	12.825	5	0.5	$4d'[5/2]_2$	73	13.449	5	1.5	$5f[3/2]_2$
33	12.857	7	0.5	$4d'[5/2]_3$	74	13.450	3	1.5	$5f[3/2]_1$
34	12.865	1	1.5	$6p[1/2]_0$	75	13.451	11	1.5	$5f[9/2]_5$
35	12.870	3	1.5	$5d[1/2]_1$	76	13.451	9	1.5	$5f[9/2]_4$
36	12.903	1	1.5	$5d[1/2]_0$	77	13.453	7	1.5	$5f[5/2]_3$
37	12.973	9	1.5	$5d[7/2]_4$	78	13.453	5	1.5	$5f[5/2]_2$
38	13.004	3	0.5	$4d'[3/2]_1$	79	13.453	5	1.5	$5g[5/2]_2$
39	13.008	7	1.5	$5d[7/2]_3$	80	13.453	7	1.5	$5g[5/2]_3$
40	13.019	5	1.5	$5d[3/2]_2$	∞	14.000	4	1.5	$[\mathrm{Zn}]4p^5$
41	13.030	1	0.5	$6s'[1/2]_0$	∞'	14.665	2	0.5	$[\mathrm{Zn}]4p^5$

Table 9: Lowest 80 levels of Kr I by energy.

i	j	β_{ij}^* [m²/eV]	f_{ij}
$4p^6$	$5s'[1/2]_1$	3.17×10^{-23}	1.50×10^{-01}
$4p^6$	$5s[3/2]_1$	4.42×10^{-23}	1.75×10^{-01}
$5p[1/2]_1$	$5d[3/2]_2$	2.52×10^{-23}	1.80×10^{-02}
$5p[1/2]_1$	$7s[3/2]_2$	1.84×10^{-23}	1.50×10^{-02}
$5s'[1/2]_0$	$5p'[1/2]_1$	1.15×10^{-21}	6.40×10^{-01}
$5s'[1/2]_0$	$5p'[3/2]_1$	1.09×10^{-21}	5.60×10^{-01}
$5s'[1/2]_0$	$6p[1/2]_1$	3.55×10^{-24}	5.30×10^{-03}
$5s'[1/2]_1$	$5p'[1/2]_0$	2.36×10^{-22}	1.40×10^{-01}
$5s'[1/2]_1$	$5p'[1/2]_1$	4.22×10^{-22}	2.00×10^{-01}
$5s'[1/2]_1$	$5p'[3/2]_1$	5.96×10^{-22}	2.60×10^{-01}
$5s'[1/2]_1$	$5p'[3/2]_2$	1.26×10^{-21}	6.00×10^{-01}
$5s'[1/2]_1$	$6p'[1/2]_0$	9.19×10^{-25}	3.00×10^{-03}
$5s'[1/2]_1$	$6p'[1/2]_1$	4.15×10^{-25}	1.30×10^{-03}
$5s'[1/2]_1$	$6p'[3/2]_1$	9.03×10^{-25}	2.80×10^{-03}
$5s'[1/2]_1$	$6p'[3/2]_2$	3.07×10^{-24}	9.70×10^{-03}
$5s[3/2]_1$	$5p'[3/2]_2$	1.20×10^{-23}	1.60×10^{-02}
$5s[3/2]_1$	$5p[1/2]_0$	2.44×10^{-22}	1.50×10^{-01}
$5s[3/2]_1$	$5p[3/2]_1$	7.01×10^{-22}	3.30×10^{-01}
$5s[3/2]_1$	$5p[3/2]_2$	3.68×10^{-22}	1.80×10^{-01}
$5s[3/2]_1$	$5p[5/2]_2$	1.31×10^{-21}	5.20×10^{-01}
$5s[3/2]_1$	$6p[1/2]_0$	1.68×10^{-24}	5.40×10^{-03}
$5s[3/2]_1$	$6p[3/2]_1$	2.28×10^{-24}	6.90×10^{-03}
$5s[3/2]_1$	$6p[3/2]_2$	1.28×10^{-24}	3.90×10^{-03}
$5s[3/2]_1$	$6p[5/2]_2$	1.60×10^{-24}	4.70×10^{-03}
$5s[3/2]_2$	$5p'[1/2]_1$	3.79×10^{-24}	5.90×10^{-03}
$5s[3/2]_2$	$5p'[3/2]_2$	8.32×10^{-25}	1.30×10^{-03}
$5s[3/2]_2$	$5p[1/2]_1$	7.15×10^{-22}	2.70×10^{-01}
$5s[3/2]_2$	$5p[3/2]_1$	5.05×10^{-23}	2.98×10^{-02}
$5s[3/2]_2$	$5p[3/2]_2$	4.41×10^{-22}	2.70×10^{-01}
$5s[3/2]_2$	$5p[5/2]_2$	2.57×10^{-22}	1.30×10^{-01}
$5s[3/2]_2$	$5p[5/2]_3$	9.93×10^{-22}	5.00×10^{-01}
$5s[3/2]_2$	$6p[1/2]_1$	4.32×10^{-25}	1.40×10^{-03}
$5s[3/2]_2$	$6p[3/2]_2$	2.06×10^{-24}	7.10×10^{-03}

Table 10: Atom impact excitation parameters for allowed transitions from ground state Kr I.
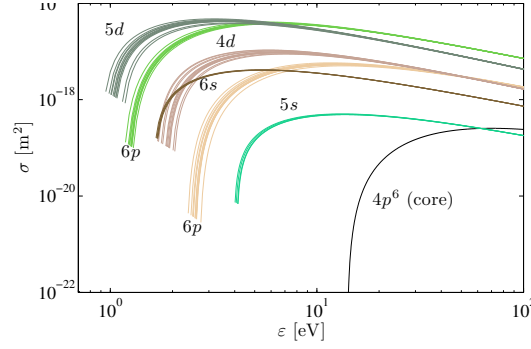
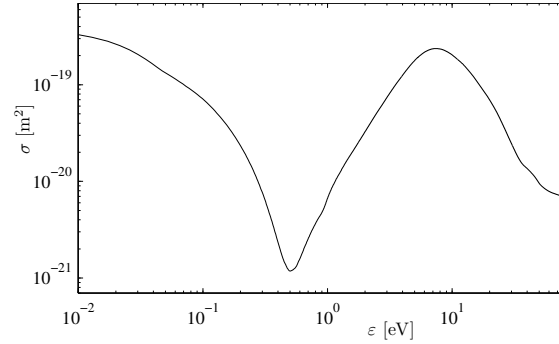Figure 6: Ionization cross sections due to electron impact for Kr I as computed by the Deutsch-Märk formalism.

Figure 7: Momentum elastic cross sections for Kr I.

4.3 Line transitions

The Einstein coefficients and oscillator strengths for allowed transitions available through the NIST database are provided in Table 4.3. The two transitions from ground state krypton have been computed by Wilkinson [34].

4.4 Validation

Initial benchmarks of the krypton CR model have been carried out for the experimental conditions provided by Glass *et al* [13]. Preliminary results are provided in Figure 8 for which only excited levels of the $5s$ manifold have been considered. Furthermore, radiation effects have been neglected.

5 Xenon

Xenon is the preferred propellant in ion thrusters including Hall thrusters due to its high Z-value and resulting I_{sp}. Due to the highly nonequilibrium conditions under which such devices operate, a detailed CR model is necessary to model the flow dynamics. Computing the required cross sections, however, is a challenge due to relativistic effects as mentioned for krypton. As such, the models that have been successfully applied to argon may

line [nm]	A [s^{-1}]	f	lower level	upper level
116.49	$2.20\times10^{+08}$	1.50×10^{-01}	$4p^6$	$5s'[1/2]_1$
123.58	$2.28\times10^{+08}$	1.75×10^{-01}	$4p^6$	$5s[3/2]_1$
427.40	$2.60\times10^{+06}$	7.10×10^{-03}	$5s[3/2]_2$	$6p[3/2]_2$
435.14	$3.20\times10^{+06}$	3.00×10^{-03}	$5s'[1/2]_1$	$6p'[1/2]_0$
436.26	$8.40\times10^{+05}$	1.40×10^{-03}	$5s[3/2]_2$	$6p[1/2]_1$
437.61	$5.60\times10^{+06}$	5.40×10^{-03}	$5s[3/2]_1$	$6p[1/2]_0$
440.00	$2.00\times10^{+06}$	9.70×10^{-03}	$5s'[1/2]_1$	$6p'[3/2]_2$
441.04	$4.40\times10^{+05}$	1.30×10^{-03}	$5s'[1/2]_1$	$6p'[1/2]_1$
442.52	$9.70\times10^{+05}$	2.80×10^{-03}	$5s'[1/2]_1$	$6p'[3/2]_1$
445.39	$7.80\times10^{+05}$	3.90×10^{-03}	$5s[3/2]_1$	$6p[3/2]_2$
446.37	$2.30\times10^{+06}$	6.90×10^{-03}	$5s[3/2]_1$	$6p[3/2]_1$
450.24	$9.20\times10^{+05}$	4.70×10^{-03}	$5s[3/2]_1$	$6p[5/2]_2$
556.22	$2.80\times10^{+05}$	1.30×10^{-03}	$5s[3/2]_2$	$5p'[3/2]_2$
557.03	$2.10\times10^{+06}$	5.90×10^{-03}	$5s[3/2]_2$	$5p'[1/2]_1$
564.96	$3.70\times10^{+05}$	5.30×10^{-03}	$5s'[1/2]_0$	$6p[1/2]_1$
587.09	$1.80\times10^{+06}$	1.60×10^{-02}	$5s[3/2]_1$	$5p'[3/2]_2$
690.47	$1.30\times10^{+06}$	1.50×10^{-02}	$5p[1/2]_1$	$7s[3/2]_2$
722.41	$1.40\times10^{+06}$	1.80×10^{-02}	$5p[1/2]_1$	$5d[3/2]_2$
758.74	$5.10\times10^{+07}$	1.50×10^{-01}	$5s[3/2]_1$	$5p[1/2]_0$
760.15	$3.10\times10^{+07}$	2.70×10^{-01}	$5s[3/2]_2$	$5p[3/2]_2$
768.52	$4.90\times10^{+07}$	1.40×10^{-01}	$5s'[1/2]_1$	$5p'[1/2]_0$
769.45	$5.60\times10^{+06}$	2.98×10^{-02}	$5s[3/2]_2$	$5p[3/2]_1$
785.48	$2.30\times10^{+07}$	6.40×10^{-01}	$5s'[1/2]_0$	$5p'[1/2]_1$
805.95	$1.90\times10^{+07}$	5.60×10^{-01}	$5s'[1/2]_0$	$5p'[3/2]_1$
810.44	$1.30\times10^{+07}$	1.30×10^{-01}	$5s[3/2]_2$	$5p[5/2]_2$
811.29	$3.60\times10^{+07}$	5.00×10^{-01}	$5s[3/2]_2$	$5p[5/2]_3$
819.01	$1.10\times10^{+07}$	1.80×10^{-01}	$5s[3/2]_1$	$5p[3/2]_2$
826.32	$3.50\times10^{+07}$	6.00×10^{-01}	$5s'[1/2]_1$	$5p'[3/2]_2$
828.11	$1.90\times10^{+07}$	2.00×10^{-01}	$5s'[1/2]_1$	$5p'[1/2]_1$
829.81	$3.20\times10^{+07}$	3.30×10^{-01}	$5s[3/2]_1$	$5p[3/2]_1$
850.89	$2.40\times10^{+07}$	2.60×10^{-01}	$5s'[1/2]_1$	$5p'[3/2]_1$
877.68	$2.70\times10^{+07}$	5.20×10^{-01}	$5s[3/2]_1$	$5p[5/2]_2$
892.87	$3.70\times10^{+07}$	2.70×10^{-01}	$5s[3/2]_2$	$5p[1/2]_1$

Table 11: Allowed transitions for Kr I available from NIST [29]. The oscillator strength is denoted by f.
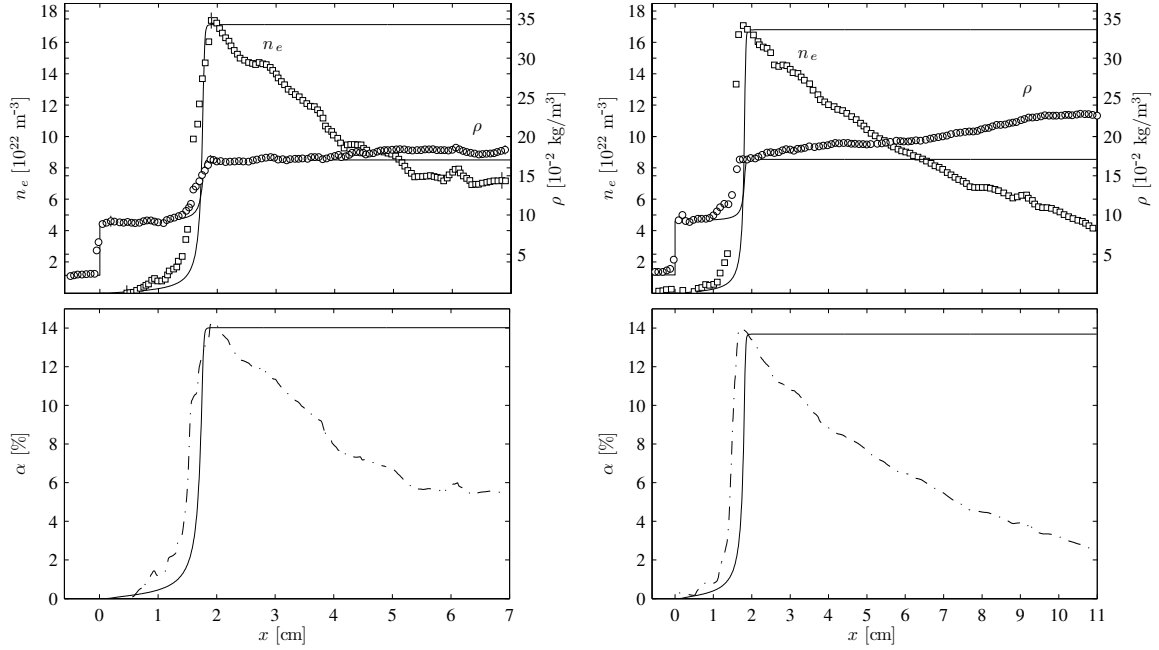
Figure 8: Heavy particle mass density and electron number density profiles (*top*) and ionization fractions (*bottom*) behind Mach 15.17 (*left*) and Mach 15.05 (*right*) shocks in pure krypton. Results shown have been obtained considering only excited levels from the $5s$ manifold while neglecting radiative processes.

breakdown and therefore caution must be exercised in their application. These models have been used as an initial base to construct out CR model and new quantum calculations which do take into account the necessary relativistic effects are promising. Our preliminary model for Xenon follows.

The effect of spin-orbit splitting of the ion due to the core angular momentum j_c (3/2 or 1/2) is more evident in Xe than Ar which leads to larger energy separation between the two groups. This effect can be seen upon comparison of the Grotrian diagrams for Xe and Ar in Figure 9. The first 80 levels are provided in Table 12.

5.1   Atom impact processes

As for argon and krypton, the formula of Drawin (Eq. 8) has been used to obtain cross sections for the allowed transitions. The parameters β_{ij}^* are provided in Table 5.1.

5.2   Electron impact processes

Zatsarinny & Bartschat [36] have computed preliminary electron impact excitation cross sections for xenon. Cross sections taken from their publications reproduced in Figures 10 and 11 show good agreement with high-resolution experiments near threshold.
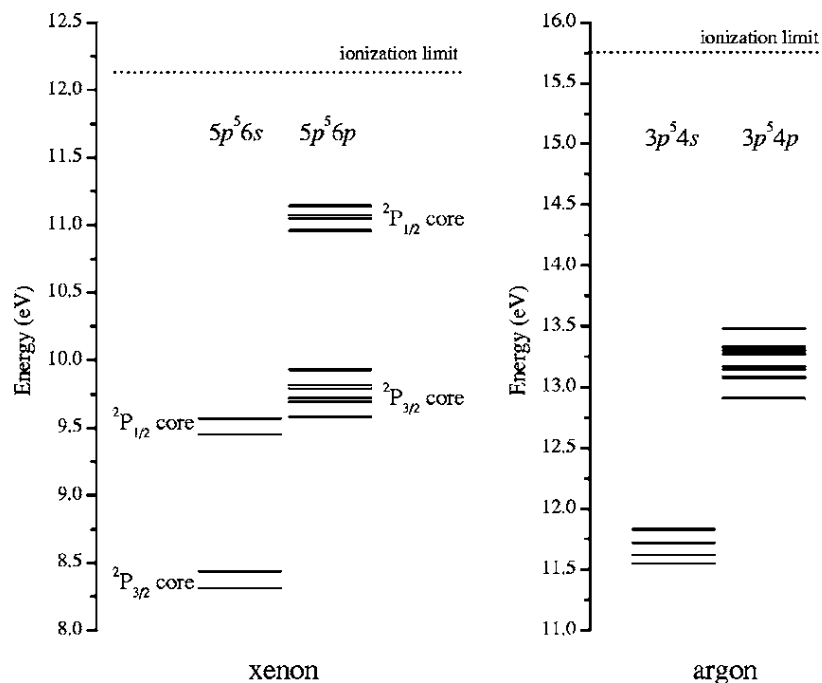
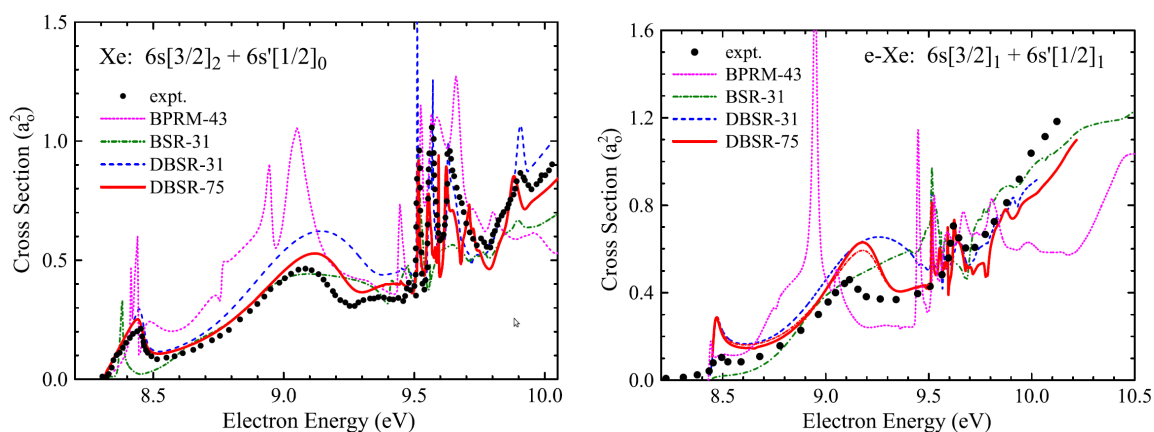Figure 9: Comparison of Xe and Ar energy lines from [16].

Figure 10: e-impact excitation cross sections to 5s manifold from ground state Xe.

| i	$\varepsilon(i)$ [eV]	g_i	j_c	$n\ell[K]_J$	i	$\varepsilon(i)$ [eV]	g_i	j_c	$n\ell[K]_J$
1	0	1	1.5	$[\text{Cd}]5p^6$	42	11.264	5	1.5	$4f[3/2]_2$
2	8.315	5	1.5	$6s[3/2]_2$	43	11.265	11	1.5	$4f[9/2]_5$
3	8.437	3	1.5	$6s[3/2]_1$	44	11.265	9	1.5	$4f[9/2]_4$
4	9.447	1	0.5	$6s'[1/2]_0$	45	11.271	7	1.5	$4f[5/2]_3$
5	9.570	3	0.5	$6s'[1/2]_1$	46	11.271	5	1.5	$4f[5/2]_2$
6	9.580	3	1.5	$6p[1/2]_1$	47	11.274	3	1.5	$8s[3/2]_1$
7	9.686	5	1.5	$6p[5/2]_2$	48	11.276	7	1.5	$4f[7/2]_3$
8	9.721	7	1.5	$6p[5/2]_3$	49	11.276	9	1.5	$4f[7/2]_4$
9	9.789	3	1.5	$6p[3/2]_1$	50	11.301	5	0.5	$5d'[5/2]_2$
10	9.821	5	1.5	$6p[3/2]_2$	51	11.338	5	0.5	$5d'[3/2]_2$
11	9.890	1	1.5	$5d[1/2]_0$	52	11.375	7	0.5	$5d'[5/2]_3$
12	9.917	3	1.5	$5d[1/2]_1$	53	11.422	3	1.5	$7d[1/2]_1$
13	9.933	1	1.5	$6p[1/2]_0$	54	11.426	3	1.5	$8p[1/2]_1$
14	9.943	9	1.5	$5d[7/2]_4$	55	11.434	5	1.5	$8p[5/2]_2$
15	9.959	5	1.5	$5d[3/2]_2$	56	11.439	1	1.5	$7d[1/2]_0$
16	10.039	7	1.5	$5d[7/2]_3$	57	11.439	7	1.5	$8p[5/2]_3$
17	10.157	5	1.5	$5d[5/2]_2$	58	11.448	3	1.5	$8p[3/2]_1$
18	10.220	7	1.5	$5d[5/2]_3$	59	11.453	5	1.5	$8p[3/2]_2$
19	10.401	3	1.5	$5d[3/2]_1$	60	11.462	9	1.5	$7d[7/2]_4$
20	10.562	5	1.5	$7s[3/2]_2$	61	11.475	1	1.5	$8p[1/2]_0$
21	10.593	3	1.5	$7s[3/2]_1$	62	11.487	7	1.5	$7d[7/2]_3$
22	10.902	3	1.5	$7p[1/2]_1$	63	11.491	5	1.5	$7d[5/2]_2$
23	10.954	5	1.5	$7p[5/2]_2$	64	11.495	3	1.5	$7d[3/2]_1$
24	10.958	3	0.5	$6p'[3/2]_1$	65	11.496	5	1.5	$7d[3/2]_2$
25	10.969	7	1.5	$7p[5/2]_3$	66	11.498	7	1.5	$7d[5/2]_3$
26	10.971	1	1.5	$6d[1/2]_0$	67	11.575	3	1.5	$5f[3/2]_1$
27	10.979	3	1.5	$6d[1/2]_1$	68	11.576	5	1.5	$5f[3/2]_2$
28	10.996	5	1.5	$7p[3/2]_2$	69	11.577	11	1.5	$5f[9/2]_5$
29	10.998	5	1.5	$6d[3/2]_2$	70	11.577	9	1.5	$5f[9/2]_4$
30	11.003	3	1.5	$7p[3/2]_1$	71	11.580	5	1.5	$9s[3/2]_2$
31	11.015	1	1.5	$7p[1/2]_0$	72	11.580	7	1.5	$5f[5/2]_3$
32	11.024	9	1.5	$6d[7/2]_4$	73	11.581	5	1.5	$5f[5/2]_2$
33	11.038	7	1.5	$6d[7/2]_3$	74	11.583	7	1.5	$5f[7/2]_3$
34	11.055	5	0.5	$6p'[3/2]_2$	75	11.583	9	1.5	$5f[7/2]_4$
35	11.065	5	1.5	$6d[5/2]_2$	76	11.583	5	1.5	$5g[5/2]_2$
36	11.069	3	0.5	$6p'[1/2]_1$	77	11.583	7	1.5	$5g[5/2]_3$
37	11.101	7	1.5	$6d[5/2]_3$	78	11.583	3	1.5	$9s[3/2]_1$
38	11.141	1	0.5	$6p'[1/2]_0$	79	11.584	11	1.5	$5g[11/2]_5$
39	11.163	3	1.5	$6d[3/2]_1$	80	11.584	13	1.5	$5g[11/2]_6$
40	11.258	5	1.5	$8s[3/2]_2$	∞	12.130	4	1.5	$[\text{Cd}]5p^5$
41	11.263	3	1.5	$4f[3/2]_1$	∞'	13.436	2	0.5	$[\text{Cd}]5p^5$

Table 12: Lowest 80 levels of Xe I by energy.
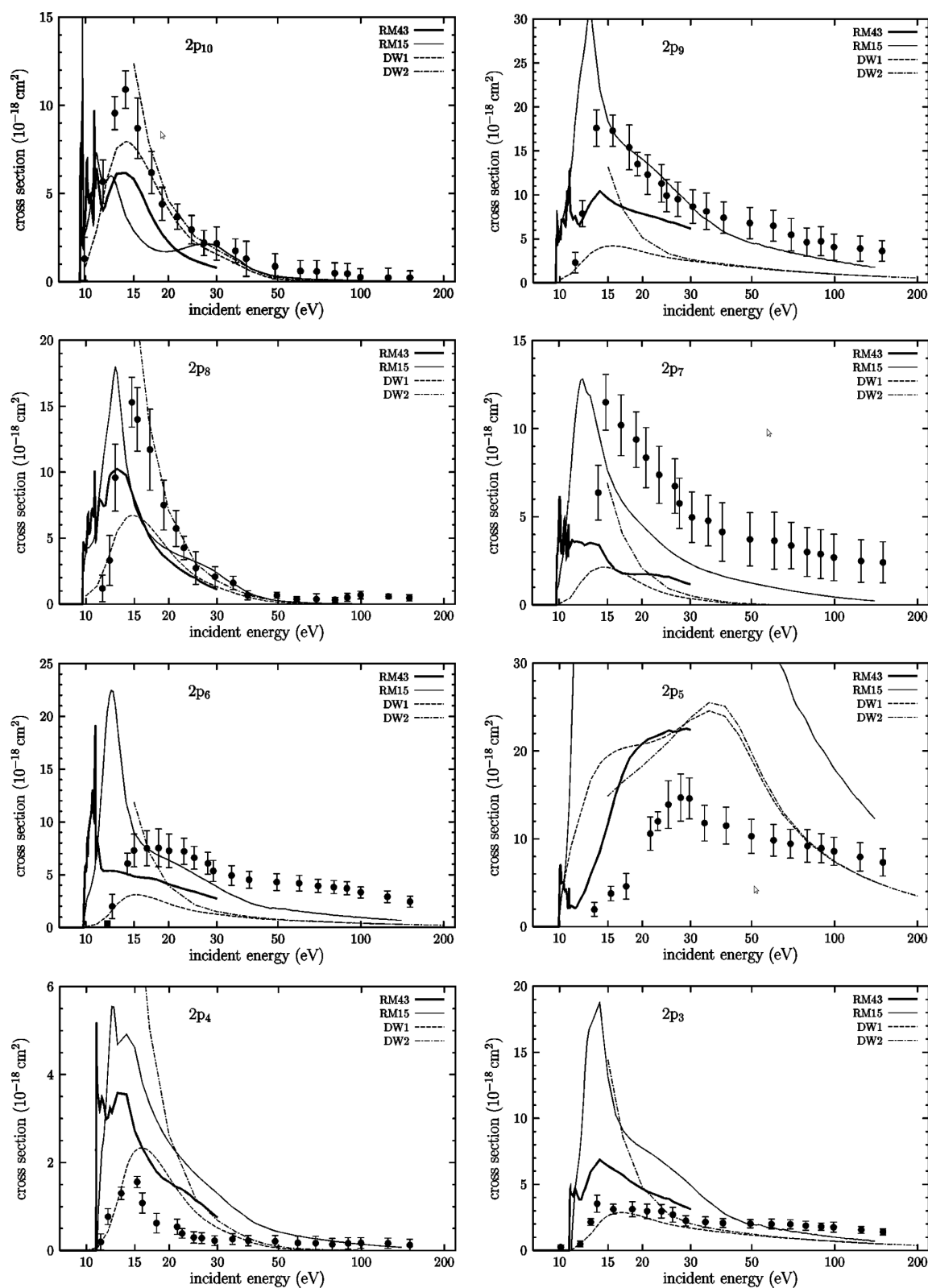
Figure 11: e-impact excitation cross sections to $5p$ manifold from ground state Xe ([1]).

i	j	β_{ij}^* [m^2/eV]	f_{ij}
$5p^6$	$5d'[3/2]_1$	3.34×10^{-23}	2.05×10^{-01}
$5p^6$	$5d[1/2]_1$	2.56×10^{-24}	9.80×10^{-03}
$5p^6$	$5d[3/2]_1$	9.06×10^{-23}	4.00×10^{-01}
$5p^6$	$6d[1/2]_1$	4.82×10^{-25}	2.50×10^{-03}
$5p^6$	$6d[3/2]_1$	1.52×10^{-23}	8.30×10^{-02}
$5p^6$	$6s'[1/2]_1$	5.41×10^{-23}	1.86×10^{-01}
$5p^6$	$6s[3/2]_1$	1.16×10^{-22}	2.73×10^{-01}
$5p^6$	$7d[1/2]_1$	3.71×10^{-24}	2.17×10^{-02}
$5p^6$	$7s[3/2]_1$	2.12×10^{-23}	9.90×10^{-02}
$5p^6$	$8s[3/2]_1$	4.20×10^{-24}	2.36×10^{-02}
$6p[5/2]_3$	$7d[7/2]_4$	8.73×10^{-23}	6.50×10^{-02}
$6s'[1/2]_0$	$7p[3/2]_1$	1.62×10^{-23}	8.60×10^{-03}
$6s[3/2]_1$	$7p[1/2]_0$	1.16×10^{-24}	2.80×10^{-03}
$6s[3/2]_2$	$6p'[1/2]_1$	3.73×10^{-25}	1.10×10^{-03}
$6s[3/2]_2$	$6p'[3/2]_2$	2.21×10^{-25}	6.40×10^{-04}
$6s[3/2]_2$	$6p[3/2]_1$	1.42×10^{-23}	6.40×10^{-03}
$6s[3/2]_2$	$7p[3/2]_2$	8.46×10^{-25}	2.30×10^{-03}
$6s[3/2]_2$	$7p[5/2]_3$	1.74×10^{-24}	4.60×10^{-03}

Table 13: Atom impact excitation parameters for allowed transitions of Xe I.

5.3   Elastic collisions

The momentum transfer cross sections for Xe have been plotted in Figure 12 [26]. These data include cross sections from [31] for energies up to 2 eV and from Gibson *et al* [11] for energies up to 50 eV. The values of Gibson were extrapolated to obtain cross sections to 100 eV.
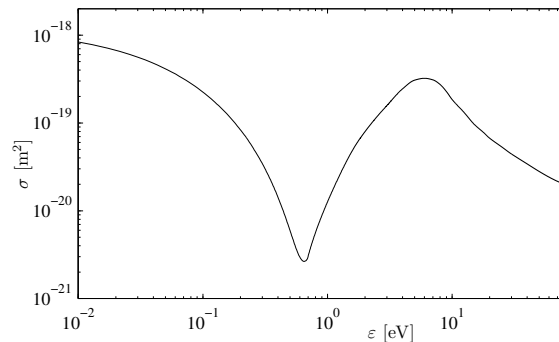

Figure 12: Momentum elastic cross sections for Xe I compiled by Mitroy [26].

5.4   Line transitions

Like Krypton, only a handful of allowed transitions for Xe I are provided in the NIST database which are given in Table 5.4. As previously mentioned, relativistic effects add complexity to *ab initio* calculations, resulting in significant uncertainty.

5.5   Validation

While simulations in Xenon have yet to be performed, we present here experimental data for future benchmarks of the model. The experimental data obtained by Ezumi *et al* [9] for a Mach 13.1 shock in pure xenon is plotted in Figure 13. Upon fitting his model to the data, Ezumi was able to determine a value of 1.8×10^{-13} m^2/eV for the xenon-xenon excitation cross section. Data has also been provided for hydrogen-xenon mixtures, from which the corresponding atom-atom excitation cross sections can be

6   Rate formulation

The cross sections must be integrated based on the distribution of particle energies in order to be applied successfully in a meaningful computation. The forward rate coefficients are computed assuming a Maxwellian electron energy distribution function (EEDF) according to

$$k = \frac{\bar{v}}{(k_{\mathrm{B}}T)^2} \int_{\varepsilon_\circ}^{\infty} \sigma(\varepsilon)\varepsilon e^{-\varepsilon/k_{\mathrm{B}}T} \; d\varepsilon \tag{40}$$

where $\varepsilon_\circ$ is the threshold energy and $\bar{v}$ is the mean thermal velocity,

$$\bar{v} = \left(\frac{8k_{\mathrm{B}}T}{\pi\mu} \right)^{1/2}, \tag{41}$$

with μ the reduced mass. The backward rates are then computed from the principle of detailed balance. For excitation processes this takes the form

$$k_{ji}^{dex} = k_{ij}^{exc} \frac{g_i}{g_j} e^{\varepsilon_{ij}/k_{\mathrm{B}}T} \tag{42}$$

where $\varepsilon_{ij} = \varepsilon_j - \varepsilon_i$ is the energy difference between the upper and lower levels. The temperature in Eq. (42) is that of the the impact species. For ionization and recombination processes, the reverse rates are also computed via detailed balance, leading to:

$$k_i^{rec} = k_i^{ion} \frac{Z_i}{Z_+ Z_e} \tag{43}$$

where Z_e is the electron partition function

line [nm]	A [s^{-1}]	f	lower level	upper level
104.38	$5.90{\times}10^{+07}$	$2.90{\times}10^{-02}$	$5p^6$	$7s'[1/2]_1$
104.71	$1.30{\times}10^{+08}$	$6.40{\times}10^{-02}$	$5p^6$	$9d[3/2]_1$
105.01	$8.50{\times}10^{+06}$	$4.20{\times}10^{-03}$	$5p^6$	$9d[1/2]_1$
105.61	$2.45{\times}10^{+08}$	$1.23{\times}10^{-01}$	$5p^6$	$8d[3/2]_1$
106.13	$1.90{\times}10^{+07}$	$9.60{\times}10^{-03}$	$5p^6$	$8d[1/2]_1$
106.82	$3.99{\times}10^{+08}$	$2.05{\times}10^{-01}$	$5p^6$	$5d'[3/2]_1$
108.54	$4.10{\times}10^{+07}$	$2.17{\times}10^{-02}$	$5p^6$	$7d[1/2]_1$
109.97	$4.34{\times}10^{+07}$	$2.36{\times}10^{-02}$	$5p^6$	$8s[3/2]_1$
111.07	$1.50{\times}10^{+08}$	$8.30{\times}10^{-02}$	$5p^6$	$6d[3/2]_1$
112.93	$4.40{\times}10^{+06}$	$2.50{\times}10^{-03}$	$5p^6$	$6d[1/2]_1$
117.04	$1.60{\times}10^{+08}$	$9.90{\times}10^{-02}$	$5p^6$	$7s[3/2]_1$
119.20	$6.20{\times}10^{+08}$	$4.00{\times}10^{-01}$	$5p^6$	$5d[3/2]_1$
125.02	$1.40{\times}10^{+07}$	$9.80{\times}10^{-03}$	$5p^6$	$5d[1/2]_1$
129.56	$2.46{\times}10^{+08}$	$1.86{\times}10^{-01}$	$5p^6$	$6s'[1/2]_1$
146.96	$2.81{\times}10^{+08}$	$2.73{\times}10^{-01}$	$5p^6$	$6s[3/2]_1$
450.10	$6.20{\times}10^{+05}$	$1.10{\times}10^{-03}$	$6s[3/2]_2$	$6p'[1/2]_1$
452.47	$2.10{\times}10^{+05}$	$6.40{\times}10^{-04}$	$6s[3/2]_2$	$6p'[3/2]_2$
462.43	$7.20{\times}10^{+05}$	$2.30{\times}10^{-03}$	$6s[3/2]_2$	$7p[3/2]_2$
467.12	$1.00{\times}10^{+06}$	$4.60{\times}10^{-03}$	$6s[3/2]_2$	$7p[5/2]_3$
480.70	$2.40{\times}10^{+06}$	$2.80{\times}10^{-03}$	$6s[3/2]_1$	$7p[1/2]_0$
711.96	$6.60{\times}10^{+06}$	$6.50{\times}10^{-02}$	$6p[5/2]_3$	$7d[7/2]_4$
796.73	$3.00{\times}10^{+05}$	$8.60{\times}10^{-03}$	$6s'[1/2]_0$	$7p[3/2]_1$
840.92	$1.00{\times}10^{+06}$	$6.40{\times}10^{-03}$	$6s[3/2]_2$	$6p[3/2]_1$

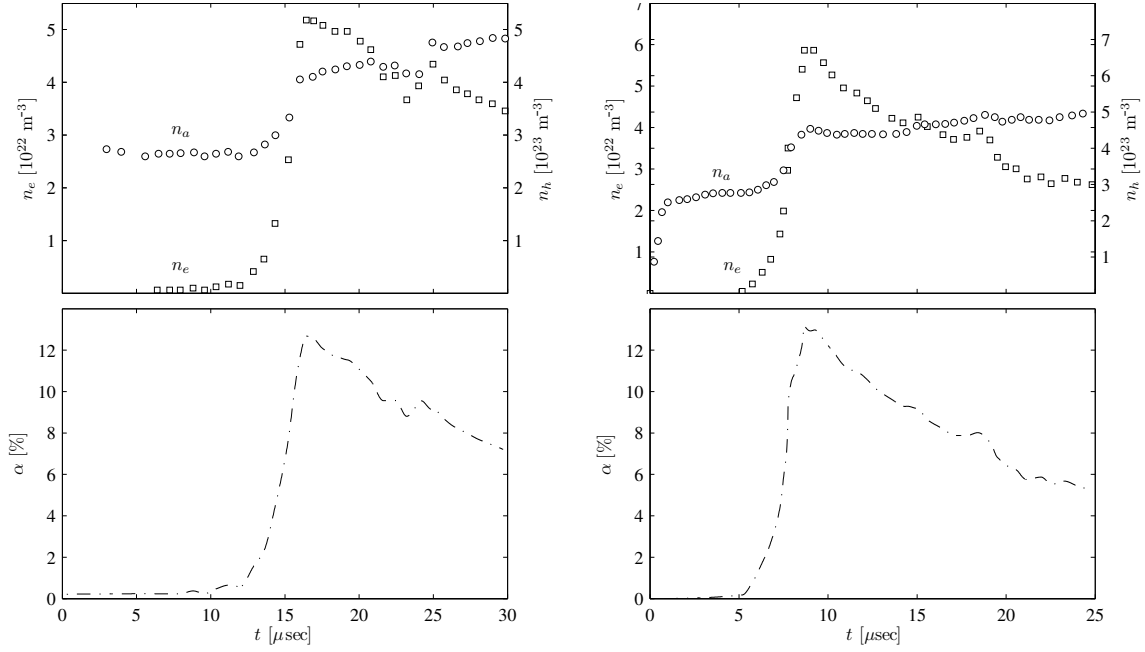Table 14: Allowed transitions for Xe I available from NIST [29]. The oscillator strength is denoted by f.

Figure 13: Number density profiles for atoms and electrons (*top*) and ionization fractions (*bottom*) behind a Mach 13.1 shock ($p = 2.0$ torr). Left profiles are for pure Xe, while right profiles are for driven gas doped with 0.17% H_2.

$$Z_e = 2 \left(\frac{2\pi m_e k_{\mathrm{B}} T_e}{h^2} \right)^{3/2} \tag{44}$$

Since the electronic states are considered separately, the ratio of partition functions for Ar and Ar^+ is simply

$$\frac{Z_i}{Z_+} \approx \frac{g_i}{g_+} e^{I_i/k_{\mathrm{B}}T} \tag{45}$$

with I_i being the ionization potential of the ith excited state, allowing Eq. (43) to be written as

$$k_i^{rec} = k_i^{ion} \frac{g_i}{g_+} \frac{1}{2} \left(\frac{h^2}{2\pi m_e k_{\mathrm{B}} T_e} \right)^{3/2} e^{I_i/k_{\mathrm{B}}T}. \tag{46}$$

Note that the exponential temperature dependence in Eq. (46) is a function of the third body—T is taken to be either the electron or heavy particle temperature for cases in which the third body is an electron or atom, respectively.

In addition to species production rates, the second moment with respect to energy is also necessary to determine the energy production rate for photorecombination (radiative capture) processes,

$$R' = \frac{\bar{v}}{(k_{\mathrm{B}}T)^2} \int_{\varepsilon_\circ}^{\infty} \sigma(\varepsilon)\varepsilon^2 e^{-\varepsilon/k_{\mathrm{B}}T} \, d\varepsilon. \tag{47}$$

In practice, all rate coefficients and their derivatives are computed *a priori* and tabulated as a function of temperature.

The model cross sections and rates used in the CR model are now described. For further details, the reader is directed to the work of Bultel *et al* [4] and Vlček [33] and the references therein.

7   Database implementation

The collisional-radiative models and theory of the preceding sections have been incorporated into a database framework that can manage and manipulate cross sections. Dubbed "`Colorado`" for <u>Col</u>lisional <u>Rad</u>iative, the database serves three main purposes. The first is a management system which organizes the multitude of cross sections in an easily accessible fashion. The second is to provide a means to compute cross sections based on semi-empirical formulas described in the preceding sections when no better alternatives are available. The third, and perhaps most critical function, is to compute reaction rates from the aggregate of cross sections, yielding a detailed kinetics database that is directly accessible to CFD solvers.

Furthermore, `Colorado` is an object-orientated (OO) framework that makes use of OO constructs to simplify the hierarchical complexity of state-specific nonequilibrium within atoms and molecules. Fine-grained OO design allows encapsulation of necessary data for electronic levels and transition lines for a more physical representation of the data, while coarse-graining of computational-intensive tasks preserves efficiency.

7.1   Structures

From a user standpoint, the code is fairly straight-forward. A user provides an input file that specifies the levels for which the kinetic rates should be computed. Here, however, we go a step beyond what is necessary for execution of the database and discuss some of the inner workings.

When the database is executed, information about the electronic levels and line transitions are read in from existing files for a given element. These data form a collection of levels and lines from which the user can extract a specific subset, based on a simple input file. The database then performs tasks including cross section calculations and rate computations for the selected subset of levels and lines. We describe the treatment for the levels and lines in the following sections.

Configuration	Term	J	Level
3s2.3p6	1S	0	0.00
3s2.3p5.(2P*<3/2>).4s	2[3/2]*	2	11.5483537
		1	11.6235920
3s2.3p5.(2P*<1/2>).4s	2[1/2]*	0	11.7231596
		1	11.8280704
3s2.3p5.(2P*<3/2>).4p	2[1/2]	1	12.90701448
3s2.3p5.(2P*<3/2>).4p	2[5/2]	3	13.07571488
		2	13.09487173
3s2.3p5.(2P*<3/2>).4p	2[3/2]	1	13.15314303
		2	13.17177687
3s2.3p5.(2P*<3/2>).4p	2[1/2]	0	13.27303726
3s2.3p5.(2P*<1/2>).4p	2[3/2]	1	13.28263817
		2	13.30222662
3s2.3p5.(2P*<1/2>).4p	2[1/2]	1	13.32785620
		0	13.47988596
3s2.3p5.(2P*<3/2>).3d	2[1/2]*	0	13.8450376
		1	13.8636677
3s2.3p5.(2P*<3/2>).3d	2[3/2]*	2	13.9034537
3s2.3p5.(2P*<3/2>).3d	2[7/2]*	4	13.9792365
		3	14.0127372
3s2.3p5.(2P*<3/2>).3d	2[5/2]*	2	14.0630263
3s2.3p5.(2P*<3/2>).5s	2[3/2]*	2	14.0682968
		1	14.0899676
3s2.3p5.(2P*<3/2>).3d	2[5/2]*	3	14.0990550
3s2.3p5.(2P*<3/2>).3d	2[3/2]*	1	14.1525142
3s2.3p5.(2P*<1/2>).3d	2[5/2]*	2	14.2136706
3s2.3p5.(2P*<1/2>).3d	2[3/2]*	2	14.2340217
3s2.3p5.(2P*<1/2>).3d	2[5/2]*	3	14.2361052
3s2.3p5.(2P*<1/2>).5s	2[1/2]*	0	14.2410268
		1	14.2550847
3s2.3p5.(2P*<1/2>).3d	2[3/2]*	1	14.3036675
3s2.3p5.(2P*<3/2>).5p	2[1/2]	1	14.46399485
3s2.3p5.(2P*<3/2>).5p	2[5/2]	3	14.49905272
		2	14.50606672
3s2.3p5.(2P*<3/2>).5p	2[3/2]	1	14.52491238
		2	14.52891256
3s2.3p5.(2P*<3/2>).5p	2[1/2]	0	14.57594785
3s2.3p5.(2P*<1/2>).5p	2[3/2]	1	14.68064940
3s2.3p5.(2P*<1/2>).5p	2[1/2]	1	14.68711731
3s2.3p5.(2P*<1/2>).5p	2[3/2]	2	14.68828937
3s2.3p5.(2P*<3/2>).4d	2[1/2]*	0	14.6936388
		1	14.71089717
3s2.3p5.(2P*<1/2>).5p	2[1/2]	0	14.73811442
3s2.3p5.(2P*<3/2>).4d	2[3/2]*	2	14.74253992
3s2.3p5.(2P*<3/2>).4d	2[7/2]*	4	14.7570507
		3	14.780511
3s2.3p5.(2P*<3/2>).4d	2[5/2]*	2	14.809271
		3	14.824297
3s2.3p5.(2P*<3/2>).6s	2[3/2]*	2	14.83881006
		1	14.84836805
3s2.3p5.(2P*<3/2>).4d	2[3/2]*	1	14.859229
3s2.3p5.(2P*<3/2>).4f	2[3/2]	1	14.9014407
		2	14.9014901
3s2.3p5.(2P*<3/2>).4f	2[9/2]	5	14.9037842
		4	14.9037893
3s2.3p5.(2P*<3/2>).4f	2[5/2]	3	14.9065882
		2	14.9066270
3s2.3p5.(2P*<3/2>).4f	2[7/2]	3	14.9090835
		4	14.9090883
3s2.3p5.(2P*<1/2>).4d	2[3/2]*	2	14.95260379
3s2.3p5.(2P*<1/2>).4d	2[5/2]*	2	14.95485109
		3	14.97152141
3s2.3p5.(2P*<1/2>).4d	2[3/2]*	1	15.00356492
3s2.3p5.(2P*<3/2>).6p	2[1/2]	1	15.0106092
3s2.3p5.(2P*<1/2>).6s	2[1/2]*	0	15.0140645
		1	15.02208738
3s2.3p5.(2P*<3/2>).6p	2[5/2]	3	15.0225900
		2	15.0258678
3s2.3p5.(2P*<3/2>).6p	2[3/2]	1	15.0339710
		2	15.0356393
3s2.3p5.(2P*<3/2>).6p	2[1/2]	0	15.0603891
3s2.3p5.(2P*<1/2>).4f	2[7/2]	3	15.0830782
		4	15.0830834
3s2.3p5.(2P*<1/2>).4f	2[5/2]	3	15.0832017
		2	15.0832446
3s2.3p5.(2P*<3/2>).5d	2[1/2]*	0	15.10054275
		1	15.11774542
3s2.3p5.(2P*<3/2>).5d	2[7/2]*	4	15.13054341
3s2.3p5.(2P*<3/2>).5d	2[3/2]*	2	15.13684751
3s2.3p5.(2P*<3/2>).5d	2[7/2]*	3	15.14592734
3s2.3p5.(2P*<3/2>).5d	2[5/2]*	2	15.1610477
		3	15.1669454
3s2.3p5.(2P*<3/2>).7s	2[3/2]*	2	15.18063262
		1	15.18550704
3s2.3p5.(2P*<3/2>).5d	2[3/2]*	1	15.1898229
3s2.3p5.(2P*<1/2>).6p	2[1/2]	1	15.2006136
3s2.3p5.(2P*<1/2>).6p	2[3/2]	1	15.2016566
		2	15.2048079
3s2.3p5.(2P*<3/2>).5f	2[3/2]	1	15.2111325
		2	15.2111752
3s2.3p5.(2P*<3/2>).5f	2[9/2]	5	15.2123191
		4	15.2123267
3s2.3p5.(2P*<3/2>).5f	2[5/2]	3	15.2138399
		2	15.2138677
3s2.3p5.(2P*<3/2>).5g	2[5/2]*	3	15.214032
		2	15.214032
3s2.3p5.(2P*<3/2>).5g	2[11/2]*	5	15.214452
		6	15.214452
3s2.3p5.(2P*<3/2>).5f	2[7/2]	3	15.2150700
		4	15.2150737
3s2.3p5.(2P*<3/2>).5g	2[7/2]*	4	15.215274
		3	15.215274
3s2.3p5.(2P*<3/2>).5g	2[9/2]*	5	15.215711
		4	15.215711
3s2.3p5.(2P*<1/2>).6p	2[1/2]	0	15.2240866
3s2.3p5.(2P*<3/2>).7p	2[1/2]	1	15.2713708
3s2.3p5.(2P*<3/2>).7p	2[5/2]	3	15.2755689
		2	15.277418
3s2.3p5.(2P*<3/2>).7p	2[3/2]	1	15.281660
		2	15.2824804
3s2.3p5.(2P*<1/2>).5d	2[3/2]*	2	15.29629228

Listing 1: Partial listing of ASCII file for NIST lines of Ar I. The files for the levels have been obtained from the NIST Atomic Spectra Database (ASD) website.

7.1.1   Electron-specific levels

The initial task of `Colorado` when first executed, is to read in the electronic levels from an ASCII files which provides the configuration name, term, J value, and energy. The partial contents of such a file is provided in listing 7.1.1. I/O support in this case is provided by the `LevelReader` class that reads in the file, and for each level, instantiates a new `Level` object. The reader returns a `Map` which contains a collection of `Level` objects, mapped to their configuration names, facilitating access to each individual level. The class `Level` parses and stores the pertinent information including configuration names, quantum numbers, and energies. A method that takes a collection of individual levels and combines them into a single averaged state is also provided. Partial code for the `LevelReader` and `Level` classes are provided in listings 1 and 2, respectively.

The ASCII files containing the NIST data for the levels are named according to the element name followed by Roman numerals for the ionization level with the file name extension `.levels`. For example, the files `ArI.levels`, `ArII.levels`, and `ArIII.levels` correspond to ground state, singly-, and doubly-ionized argon, respectively.

Listing 1: LevelReader class

```java
public class LevelReader
{
    public static Map<String, Level> read(String specie){ ... }
}
```

Listing 2: Level class

```java
public class Level
{
    /** Unicode descriptor */
    public String name;
    /** NIST-assigned configuration */
    public String config;
    /** NIST-assigned term */
    public String term;
    /** Valence shell */
    public String nℓ;

    /** Index of this level */
    public int index;
    /** Principal quantum number */
    public int n;
    /** Orbital angular momentum quantum number */
    public int ℓ;
    /** Total orbital angular momentum quantum number */
    public int L;
    /**  */
    public int K;
    /** Total angular momentum quantum number */
    public double J;
    /** Statistical weight */
    public double g;
    /** Statistical weight of ionized level */
    public double gp;
    /** Number of optical electrons */
    public double ξ;
    /** Excitation energy in eV */
    public double ε;
    /** Ionization potential */
    public double IP;
    /** Core quantum number */
    public double jc;
    /** Primed (jc=1/2) or not (jc=3/2) */
    public boolean primed;

    public boolean combined;
    public Level[] group;

    public Level(){}

    public static Level parseNIST(String config, String term, double J, double ε){ ... }
    public static String getName(String config, String term, int J){ ... }
    public static Level combine(String name, Map<String, Level> levels){ ... }
    public static String transition_type(Level ℓ1, Level ℓ2){ ... }
    public static Level getCopy(Level level){ ... }
}
```

7.1.2   Line transitions

In much the same way as a collection of `Level` objects is created from an ASCII file of NIST levels, a collection of `Line` objects is created from a file of NIST transitions lines. This is accomplished by the `LineReader` class given in listing 3. It takes as an argument the collection of `Level` objects so that when a `Line` object is instantiated, it includes the necessary information about the transition such as the wavelength as well as pointers to the actual upper and lower `Level` objects. This facilitates access to the level information when performing operations involving the transitions. As sample listing of the NIST transition lines is provided in listing 7.1.2 and the form of the `Line` class is given in listing 4.

Listing 3: LineReader class

```
public class LineReader
{
    public static Map<String, Line> read(String specie, Map<String, Level> levels){ ... }
}
```

Listing 4: Line class

```
public class Line
{
    /** Transition wavelength [m] */
    public double λ;
    /** Einstein coefficient */
    public double A;
    /** Oscillator strength */
    public double f;
    /** Lower level */
    public Level lower;
    /** Upper level */
    public Level upper;

    public Line(){}

    public static Map<String, Line> parseNIST(String path, Map<String, Level> levels){ ... }
    public static Line getCopy(Line line){ ... }
}
```

Ritz Wavelength Vac (nm)	Transition Wavenumber (cm-1)	Aki s^-1	fik	Acc.	Ei (eV)	Ek (eV)	Configurations	Terms	Ji Jk	gi - gk	Type
86.6800	115366.866	3.13e+08	1.06e-01	C+	0.00	14.3036675	3s2.3p6 - 3s2.3p5.(2P*<1/2>).3d	1S - 2[3/2]*	0 - 1	1 - 3	
86.9754	114975.019	3.50e+07	1.19e-02	C	0.00	14.2550847	3s2.3p6 - 3s2.3p5.(2P*<1/2>).5s	1S - 2[1/2]*	0 - 1	1 - 3	
87.6058	114147.732	2.70e+08	9.32e-02	C+	0.00	14.1525142	3s2.3p6 - 3s2.3p5.(2P*<3/2>).3d	1S - 2[3/2]*	0 - 1	1 - 3	
87.9947	113643.260	7.7e+07	2.7e-02	C+	0.00	14.0899676	3s2.3p6 - 3s2.3p5.(2P*<3/2>).5s	1S - 2[3/2]*	0 - 1	1 - 3	
104.8220	95399.8276	5.1e+08	2.5e-01	C+	0.00	11.8280704	3s2.3p6 - 3s2.3p5.(2P*<3/2>).4s	1S - 2[1/2]*	0 - 1	1 - 3	
106.6660	93750.5978	1.19e+08	6.09e-02	C+	0.00	11.6235920	3s2.3p6 - 3s2.3p5.(2P*<3/2>).4s	1S - 2[3/2]*	0 - 1	1 - 3	
340.6180	29349.977	3.9e+05	2.3e-04	D	11.8280704	15.4670036	3s2.3p5.(2P*<1/2>).4s - 3s2.3p5.(2P*<1/2>).7p	2[1/2]* - 2[1/2]	1 - 0	3 - 1	
346.1078	28884.456	6.7e+04	2.0e-04	D	11.6235920	15.2048079	3s2.3p5.(2P*<3/2>).4s - 3s2.3p5.(2P*<1/2>).6p	2[3/2]* - 2[3/2]	1 - 2	3 - 5	
355.4305	28126.857	2.7e+05	5.1e-04	D	11.5483537	15.0356393	3s2.3p5.(2P*<3/2>).4s - 3s2.3p5.(2P*<3/2>).6p	2[3/2]* - 2[3/2]	2 - 2	5 - 5	
356.3286	28055.972	1.2e+05	6.9e-04	D	11.7231596	15.2016566	3s2.3p5.(2P*<1/2>).4s - 3s2.3p5.(2P*<1/2>).6p	2[1/2]* - 2[3/2]	0 - 1	1 - 3	
356.7656	28021.607	1.1e+05	2.9e-04	D	11.5483537	15.0225900	3s2.3p5.(2P*<3/2>).4s - 3s2.3p5.(2P*<3/2>).6p	2[3/2]* - 2[5/2]	2 - 3	5 - 7	
357.2295	27985.216	5.1e+05	3.3e-04	D	11.8280704	15.2977948	3s2.3p5.(2P*<1/2>).4s - 3s2.3p5.(2P*<3/2>).7p	2[1/2]* - 2[1/2]	1 - 0	3 - 1	
360.6522	27719.640	7.6e+05	4.9e-04	D	11.6235920	15.0603891	3s2.3p5.(2P*<3/2>).4s - 3s2.3p5.(2P*<3/2>).6p	2[3/2]* - 2[1/2]	1 - 0	3 - 1	
363.2683	27520.019	6.6e+04	2.2e-04	D	11.6235920	15.0356393	3s2.3p5.(2P*<3/2>).4s - 3s2.3p5.(2P*<3/2>).6p	2[3/2]* - 2[3/2]	1 - 2	3 - 5	
363.4460	27506.563	1.3e+05	2.6e-04	D	11.6235920	15.0339710	3s2.3p5.(2P*<3/2>).4s - 3s2.3p5.(2P*<3/2>).6p	2[3/2]* - 2[3/2]	1 - 1	3 - 3	
364.3116	27441.207	2.4e+04	8.0e-05	D	11.6235920	15.0258678	3s2.3p5.(2P*<3/2>).4s - 3s2.3p5.(2P*<3/2>).6p	2[3/2]* - 2[5/2]	1 - 2	3 - 5	
364.9832	27390.719	8.0e+05	5.3e-04	D	11.8280704	15.2240866	3s2.3p5.(2P*<1/2>).4s - 3s2.3p5.(2P*<1/2>).6p	2[1/2]* - 2[1/2]	1 - 0	3 - 1	
365.9529	27318.138	4.4e+04	8.8e-05	D	11.6235920	15.0106092	3s2.3p5.(2P*<3/2>).4s - 3s2.3p5.(2P*<3/2>).6p	2[3/2]* - 2[3/2]	1 - 1	3 - 3	
367.0670	27235.226	3.1e+04	1.0e-04	D	11.8280704	15.2048079	3s2.3p5.(2P*<1/2>).4s - 3s2.3p5.(2P*<1/2>).6p	2[1/2]* - 2[3/2]	1 - 2	3 - 5	
367.5235	27201.397	4.9e+04	9.9e-05	D	11.8280704	15.2006136	3s2.3p5.(2P*<1/2>).4s - 3s2.3p5.(2P*<3/2>).6p	2[1/2]* - 2[3/2]	1 - 1	3 - 3	
377.0369	26515.071	7.0e+04	4.5e-04	D	11.7231596	15.0106092	3s2.3p5.(2P*<1/2>).4s - 3s2.3p5.(2P*<3/2>).6p	2[1/2]* - 2[1/2]	0 - 1	1 - 3	
383.4678	26070.410	7.5e+05	5.5e-04	D	11.8280704	15.0603891	3s2.3p5.(2P*<1/2>).4s - 3s2.3p5.(2P*<3/2>).6p	2[1/2]* - 2[1/2]	1 - 0	3 - 1	
389.4660	25668.908	5.7e+04	1.3e-04	D	11.8280704	15.0106092	3s2.3p5.(2P*<1/2>).4s - 3s2.3p5.(2P*<3/2>).6p	2[1/2]* - 2[3/2]	1 - 1	3 - 3	
394.7505	25325.2908	5.6e+04	1.3e-04	C	11.5483537	14.68828937	3s2.3p5.(2P*<3/2>).4s - 3s2.3p5.(2P*<1/2>).5p	2[3/2]* - 2[3/2]	2 - 2	5 - 5	
394.8979	25315.8375	4.55e+05	6.39e-04	C	11.5483537	14.68711731	3s2.3p5.(2P*<3/2>).4s - 3s2.3p5.(2P*<1/2>).5p	2[3/2]* - 2[1/2]	2 - 1	5 - 3	
404.4418	24718.4530	3.33e+05	1.36e-03	C	11.6235920	14.68828937	3s2.3p5.(2P*<3/2>).4s - 3s2.3p5.(2P*<1/2>).5p	2[3/2]* - 2[3/2]	1 - 2	3 - 5	
404.5965	24708.9997	4.1e+04	1.0e-04	C	11.6235920	14.68711731	3s2.3p5.(2P*<3/2>).4s - 3s2.3p5.(2P*<1/2>).5p	2[3/2]* - 2[1/2]	1 - 1	3 - 3	
405.4526	24656.8325	2.7e+04	6.7e-05	C	11.6235920	14.68064940	3s2.3p5.(2P*<3/2>).4s - 3s2.3p5.(2P*<3/2>).5p	2[3/2]* - 2[3/2]	1 - 1	3 - 3	
415.8591	24039.8301	1.40e+06	3.63e-03	C	11.5483537	14.52891256	3s2.3p5.(2P*<3/2>).4s - 3s2.3p5.(2P*<3/2>).5p	2[3/2]* - 2[3/2]	2 - 2	5 - 5	
416.4180	24007.5664	2.88e+05	4.49e-04	C	11.5483537	14.52491238	3s2.3p5.(2P*<3/2>).4s - 3s2.3p5.(2P*<3/2>).5p	2[3/2]* - 2[3/2]	2 - 1	5 - 3	
418.1884	23905.9323	5.61e+05	4.41e-03	C	11.7231596	14.68711731	3s2.3p5.(2P*<1/2>).4s - 3s2.3p5.(2P*<1/2>).5p	2[1/2]* - 2[1/2]	0 - 1	1 - 3	
419.0713	23855.5659	2.80e+05	7.38e-04	C	11.5483537	14.50606672	3s2.3p5.(2P*<3/2>).4s - 3s2.3p5.(2P*<3/2>).5p	2[3/2]* - 2[5/2]	2 - 2	5 - 5	
419.1029	23853.7651	5.39e+05	4.26e-03	C	11.7231596	14.68064940	3s2.3p5.(2P*<1/2>).4s - 3s2.3p5.(2P*<3/2>).5p	2[1/2]* - 2[3/2]	0 - 1	1 - 3	
419.8317	23812.3575	2.57e+06	2.26e-03	C	11.6235920	14.57594785	3s2.3p5.(2P*<3/2>).4s - 3s2.3p5.(2P*<3/2>).5p	2[3/2]* - 2[1/2]	1 - 0	3 - 1	
420.0675	23798.9942	9.67e+05	3.58e-03	C	11.5483537	14.49052272	3s2.3p5.(2P*<3/2>).4s - 3s2.3p5.(2P*<3/2>).5p	2[3/2]* - 2[5/2]	2 - 3	5 - 7	
425.1185	23516.2334	1.11e+05	1.81e-04	C	11.5483537	14.46399485	3s2.3p5.(2P*<3/2>).4s - 3s2.3p5.(2P*<3/2>).5p	2[3/2]* - 2[1/2]	2 - 1	5 - 3	
425.9362	23471.0894	3.98e+06	3.61e-03	C	11.8280704	14.73811442	3s2.3p5.(2P*<1/2>).4s - 3s2.3p5.(2P*<1/2>).5p	2[1/2]* - 2[1/2]	1 - 0	3 - 1	
426.6287	23432.9923	3.12e+05	1.42e-03	C	11.6235920	14.52891256	3s2.3p5.(2P*<3/2>).4s - 3s2.3p5.(2P*<3/2>).5p	2[3/2]* - 2[3/2]	1 - 2	3 - 5	
427.2169	23400.7286	7.97e+05	2.18e-03	C	11.6235920	14.52491238	3s2.3p5.(2P*<3/2>).4s - 3s2.3p5.(2P*<3/2>).5p	2[3/2]* - 2[3/2]	1 - 1	3 - 3	
430.0101	23248.7281	3.77e+05	1.74e-03	C	11.6235920	14.50606672	3s2.3p5.(2P*<3/2>).4s - 3s2.3p5.(2P*<3/2>).5p	2[3/2]* - 2[5/2]	1 - 2	3 - 5	
433.3561	23069.2232	5.68e+05	2.67e-03	C	11.8280704	14.68828937	3s2.3p5.(2P*<1/2>).4s - 3s2.3p5.(2P*<1/2>).5p	2[1/2]* - 2[3/2]	1 - 2	3 - 5	
433.5338	23059.7699	3.87e+05	1.09e-03	C	11.8280704	14.68711731	3s2.3p5.(2P*<1/2>).4s - 3s2.3p5.(2P*<1/2>).5p	2[1/2]* - 2[1/2]	1 - 1	3 - 3	
434.5168	23007.6027	2.97e+05	8.41e-04	C	11.8280704	14.68064940	3s2.3p5.(2P*<1/2>).4s - 3s2.3p5.(2P*<3/2>).5p	2[1/2]* - 2[3/2]	1 - 1	3 - 3	
436.3795	22909.3956	1.2e+04	3.4e-05	D	11.6235920	14.46399485	3s2.3p5.(2P*<3/2>).4s - 3s2.3p5.(2P*<3/2>).5p	2[3/2]* - 2[1/2]	1 - 1	3 - 3	
442.3994	22597.6612	7.3e+03	6.4e-05	D	11.7231596	14.52491238	3s2.3p5.(2P*<1/2>).4s - 3s2.3p5.(2P*<3/2>).5p	2[1/2]* - 2[3/2]	0 - 1	1 - 3	
451.0733	22163.1277	1.18e+06	1.20e-03	C	11.8280704	14.57594785	3s2.3p5.(2P*<1/2>).4s - 3s2.3p5.(2P*<3/2>).5p	2[1/2]* - 2[1/2]	1 - 0	3 - 1	

Listing 2: Partial listing of ASCII file for NIST lines of Ar I.

7.2   Input

Once the collections of levels and lines have been formed, an input file provided by the user specifies the levels of particular interest. A sample input file for ArI is provided in listing 7.2. This particular file tells 'Colorado to use only the first 31 levels to construct the database. Groups of levels can also be defined by including incomplete configurations such as 4p or 5 which would find and combine all available levels with principle quantum numbers $n = 4$ and $\ell = 1$ for the former and $n = 5$ for the latter. The reader together with the files are associated with the namespace colorado.database.nist.levels. The ordering of the levels in the input file is important since it determines the ordering of the rates output by the code. It is not a requirement for the levels to be energy ordered or term ordered. The input file is Unicode in that it allows sub- and superscripts.

```
3p⁶
4s[3/2]₂
4s[3/2]₁
4s'[1/2]₀
4s'[1/2]₁
4p[1/2]₁
4p[5/2]₃
4p[5/2]₂
4p[3/2]₁
4p[3/2]₂
4p[1/2]₀
4p'[3/2]₁
4p'[3/2]₂
4p'[1/2]₁
4p'[1/2]₀
3d[1/2]₀
3d[1/2]₁
3d[3/2]₂
3d[7/2]₄
3d[7/2]₃
3d[5/2]₂
5s[3/2]₂
5s[3/2]₁
3d[5/2]₃
3d[3/2]₁
3d'[5/2]₂
3d'[3/2]₂
3d'[5/2]₃
5s'[1/2]₀
5s'[1/2]₁
3d'[3/2]₁
```

Listing 3: A sample input file for levels of Ar I. The file allows the user to communicate to Colorado which levels to include in the CR database. Unicode characters allow clear configuration descriptions and are easily handled by Java.

7.3   Rate calculations

Calculation of reaction rates from the cross sections has been implemented in Colorado based on Maxwellian distributions of both the heavy particle and electron energies. With the list of user-defined levels, the code computes the necessary rates for each of the possible processes and then stores them as a function of temperature in separate files, numbered according to their position in the user-defined input file.

7.4   Orgnaization

The cross section data is currently (and quite tentatively) organized into the following namespaces. Files such as ArI.levels and ArI.lines are maintained within the col-

orado.database.nist.levels and colorado.database.nist.lines namespaces. User input files are located in the colorado.config namespace such as the example included in listing 7.2. The actual cross sections are located according to the element name and process type. For specific models, the namespaces are labeled accordingly such as colorado.database.argon.deutsch and colorado.database.argon.zatsarinny for electron-impact ionization model of Deutsch *et al* and electron-impact excitation model of Zatsarinny & Bartschat. While these models are the most accurate included in the database, transitions for only lower-lying levels are available and therefore Drawin's cross sections are used to complete the missing information. This is handled in Colorado by first looking into the locations of the specific models to see if data is available, and then switching to the general models when the data cannot be found.

```
colorado
colorado.config
colorado.database.argon.atomic_excitation
colorado.database.argon.atomic_ionization
colorado.database.argon.deutsch
colorado.database.argon.elastic
colorado.database.argon.electronic_excitation
colorado.database.argon.electronic_ionization
colorado.database.argon.radiativerecombination
colorado.database.argon.zatsarinny
colorado.database.argon.zatsarinny_osc
colorado.database.krypton.atomic_excitation
colorado.database.krypton.atomic_ionization
colorado.database.krypton.deutsch
colorado.database.krypton.elastic
colorado.database.krypton.electronic_excitation
colorado.database.krypton.zatsarinny
colorado.database.nist.levels
colorado.database.nist.lines
colorado.database.xenon.atomic_excitation
colorado.database.xenon.atomic_ionization
colorado.database.xenon.deutsch
colorado.database.xenon.elastic
```

Listing 4: Organizational structure of the code in terms of namespaces.

8   Conclusions and future work

Collsional-Radiative models for the noble gases have been detailed which included atom- and electron-impact processes as well as radiative processes. These models are intended to support plasmadynamic simulations under conditions of high non-equilibrium. The data has been presented in terms of angle-integrated cross sections where we have no assumption of the distribution function has been assumed. This leaves open the possibility to compute the CR rates using an arbitrary distribution function, including a bin approach.

While detailed validation has been provided for argon, results for krypton and xenon are still preliminary. Work is currently underway to increase the level of sophistication. These models will be refined and benchmarked against further experimental data, including expansion flows in which radiative processes dominate.

References

[1] K. Bartschat, A. Dasgupta, and D. H. Madison. Close-coupling and distorted-wave calculations for electron-impact excitation of the $5p^56p$ states of xenon. *Phys. Rev. A*, 69:062706, 2004.

[2] M. P. F. Bristow. An experimental determination of the polarizability for singly ionized argon. (158), April 1971.

[3] S. J. Buckman, P. Hammond, G. C. King, and F. H. Read. High resolution electron-impact excitation functions of metastable states of neon, argon, krypton and xenon. *J. Phys. B: At. Mol. Phys.*, 16:4219–4236, 1983.

[4] A. Bultel, B. van Ootegem, A. Bourdon, and P. Vervisch. Influence of Ar_2^+ in an argon collisional-radiative model. *Phys. Rev. E*, 65:1–16, 2002.

[5] Jean-Luc Cambier. Numerical simulations of a nonequilibrium argon plasma in a shock-tube experiment. In *Proceedings of the 22nd Fluid Dynamics, Plasma Dynamics, and Lasers Conference*, pages 1–20, Honolulu, HI, June 1991. AIAA.

[6] H. Deutsch, K. Becker, A. N. Grum-Grzhimailo, K. Bartschat, H. Summers, M. Probst, S. Matt-Leubner, and T. D. Mark. Calculated cross sections for the electron-impact ionization of excited argon atoms using the DM formalism. *Int. J. Mass Spectrom. Ion Process.*, 233:39–43, 2004.

[7] H. Deutsch, K. Becker, S. Matt, and T. D. Märk. Calculated cross sections for the electron-impact ionization of metastable atoms. *J. Phys. B: At. Mol. Opt. Phys.*, 32:4249–4259, 1999.

[8] H. Deutsch, K. Becker, S. Matt, and T. D. Märk. Theoretical determination of absolute electron-impact ionization cross sections of molecules. *Int. J. Mass Spectrom. Ion Process.*, 197:37–69, 2000.

[9] H. Ezumi, M. Kawamura, and N. Gohda. Shock-tube measurements of the excitational cross-section in xenon-hydrogen mixture. *J. Phys. Soc. Jpn.*, 53(2):1731–1737, 1984.

[10] H. H. Fleischmann and R. C. Dehmel. On Drawin's formula for ionization in atom-atom collisions. *Z. Physik*, 252:435–442, 1972.

[11] J. C. Gibson, D. R. Lun, L. J. Allen, R. P. McEachran, L. A. Parcell, and S. J. Buckman. Low-energy electron scattering from xenon. *J. Phys. B: At. Mol. Opt. Phys.*, 31:3949–3964, 1998.

[12] I. I. Glass and W. S. Liu. Effects of hydrogen impurities on shock structure and stability in ionizing monatomic gases. Part 1. Argon. *J. Fluid Mech.*, 84(1):55–77, 1978.

[13] I. I. Glass, W. S. Liu, and F. C. Tang. Effects of hydrogen impurities on shock structure and stability in ionizing monatomic gases: 2. Krypton. *Can. J. Phys.*, 55:1269–1279, 1977.

[14] K. E. Harwell and R. C. Jahn. Initial ionization rates in shock-heated argon, krypton, and xenon. *Phys. Fluids*, 7(214):1554, 1964.

[15] Paul O. Haugsjaa and Robert C. Amme. Ionization and metastable excitation in low-energy collisions of ground state argon atoms. *J. Chem. Phys.*, 52:4874–48??, 1970.

[16] R. O. Jung, J. B. Boffard, L. W. Anderson, and C. C. Lin. Electron-impact excitation cross sections from the xenon $j = 2$ metastable level. *Phys. Rev. A*, 72:022723, 2005.

[17] M. G. Kapper and J.-L. Cambier. Ionizing shocks in argon. part i: Collisional-radiative model and steady-state structure. *J. Appl. Phys.*, 109(11):113308, 2011.

[18] M. G. Kapper and J.-L. Cambier. Ionizing shocks in argon. part ii: Transient and multi-dimensional effects. *J. Appl. Phys.*, 109(11):113309, 2011.

[19] K. Katsonis and H. W. Drawin. Transition probabilities for argon(I). *J. Quant. Spectrosc. Radiat. Transfer*, 23:1–55, 1980.

[20] A. J. Kelly. Atom-atom ionization cross sections of the noble gases—argon, krypton, and xenon. *J. Chem. Phys.*, 45:1723, 1966.

[21] R. P. McEachran and A. D. Stauffer. Relativistic effects in low-energy electron-argon scattering. *Aust. J. Phys.*, 50:511–524, 1997.

[22] R. P. McEachran and A. D. Stauffer. Elastic scattering of electrons from krypton. *J. Phys. B: At. Mol. Opt. Phys.*, 36:3977–3984, 2003.

[23] T. I. McLaren and R. M. Hobson. Initial ionization rates in shock-heated argon, krypton, and xenon. *Phys. Fluids*, 11:2152, 1968.

[24] M. Merilo and E. J. Morgan. Ionization rates behind shock waves in argon. *J. Chem. Phys.*, 52:2192, 1970.

[25] J. Mitroy. The momentum transfer cross sections for krypton. *Phys. Scr.*, 43:19–25, 1990.

[26] J. Mitroy. Xe momentum transfer, June 2011.

[27] E. J. Morgan and R. D. Morrison. Ionization rates behind shock waves in argon. *Phys. Fluids*, 8:1608, 1965.

[28] A. Nicklass, M. Dolg, H. Stoll, and H. Preuss and. *Ab initio* energy-adjusted pseudopotentials for the noble gases Ne through Xe: Calculation of atomic dipole and quadrupole polarizabilities. *J. Chem. Phys.*, 102(22):8942–8952, June 1995.

[29] Yu. Ralchenko, A. E. Kramida, J. Reader, and NIST ASD Team. NIST atomic spectra database (version 3.1.5). Technical report, NIST, 2008.

[30] R. Scott Schappe, M. Bruce Schulman, L. W. Anderson, and Chun C. Lin. Measurement of cross sections for electron-impact excitation into the metastable levels of argon and number densities of metastable argon atoms. *Phys. Rev. A*, 50(1):444–461, 1994.

[31] B. Schmidt, K. Berkhan, B. Götz, and M. Müller. New experimental techniques in the study of electron swarms in gases and their impact on the determination of low energy electron scattering cross sections. *Phys. Scr.*, T53:30–42, 1994.

[32] H. Straub, P. Renault, B. Lindsay, K. Smith, and R. Stebbings. Measurement of electron-impact excitation cross sections out of metastable levels of argon and comparison with ground-state excitation. *Phys. Rev. A*, 52:1115, 1995.

[33] J. Vlček. A collisional-radiative model applicable to argon discharges over a wide range of conditions. I: Formualtion and basic data. *J. Phys. D: Appl. Phys.*, 22:623–631, 1989.

[34] P. G. Wilkinson. Oscillator strengths of the resonance lines of the rare gases—I. Krypton. *Journal of Quantitative Spectroscopy and Radiative Transfer*, 5(2):503–510, 1965.

[35] O. Zatsarinny and K. Bartschat. *B*-spline Breit-Pauli *R*-matrix calculations for electron collisions with argon atoms. *J. Phys. B: At. Mol. Opt. Phys.*, 37:4693–4703, 2004.

[36] O. Zatsarinny and K. Bartschat. Benchmark calculations for near-threshold electron-impact excitation of krypton and xenon atoms. *J. Phys. B: At. Mol. Opt. Phys.*, 43:074031, 2010.

[37] Ya. B. Zel'dovich and Yu. P. Raizer. *Physics of Shock Waves and High Temperature Hydrodynamic Phenomena*. Dover Publications, Inc., New York, third edition, 2002.